ARTICLES
https://doi.org/10.1038/s41593-018-0276-0

nature neuroscience

Corrected: Publisher Correction

Motor primitives in space and time via targeted gain modulation in cortical networks

Jake P. Stroud[1*], Mason A. Porter[2,3,4], Guillaume Hennequin[5] and Tim P. Vogels[1]

Motor cortex (M1) exhibits a rich repertoire of neuronal activities to support the generation of complex movements. Although recent neuronal-network models capture many qualitative aspects of M1 dynamics, they can generate only a few distinct movements. Additionally, it is unclear how M1 efficiently controls movements over a wide range of shapes and speeds. We demonstrate that modulation of neuronal input–output gains in recurrent neuronal-network models with a fixed architecture can dramatically reorganize neuronal activity and thus downstream muscle outputs. Consistent with the observation of diffuse neuromodulatory projections to M1, a relatively small number of modulatory control units provide sufficient flexibility to adjust high-dimensional network activity using a simple reward-based learning rule. Furthermore, it is possible to assemble novel movements from previously learned primitives, and one can separately change movement speed while preserving movement shape. Our results provide a new perspective on the role of modulatory systems in controlling recurrent cortical activity.

Motor cortex is one of the final cortical outputs to downstream spinal motor neurons[1], and it is fundamental for controlling voluntary movements[2–4]. During movement execution, M1 exhibits complex, multiphasic firing-rate transients that return to baseline after movement completion[4]. Recent studies have provided some understanding of how these complex, single-neuron patterns of activity relate to intended movements[4–6]. It has been illuminating to view motor cortex as a dynamical system in which preparatory activity sets the initial condition for the system, whose subsequent dynamics drive the desired muscle activity[7,8]. From this perspective, the complex firing-rate dynamics provide a flexible basis set for the generation of movements[9].

Several recurrent neuronal-network models have been developed to capture M1 activity during movement execution[10,11]. These models rely on strong recurrent connectivity that is optimized for the neuronal dynamics to be qualitatively similar to M1 activity during movement execution. However, these models cannot explain how new movements can be constructed or how their static architecture allows variations in both output trajectories and speed.

A possible mechanism for effectively switching neuronal activity, and consequently downstream muscle activity, to generate different movements (Fig. 1a) is to adjust the intrinsic gain—that is, the input–output sensitivity—of each neuron so that they engage more (or less) actively in the recurrent neuronal dynamics[12–18]. Indeed, neuromodulation in M1 can cause such changes in neuronal responsiveness[19,20], and gain modulation of both neurons in M1[13] and spinal motor neurons[21,22] has been linked experimentally to skill acquisition and optimization of muscular control.

Here we study the effects of gain modulation in recurrent neuronal-network models of motor cortex. We show that individually modulating each neuron's gain allows the models to learn a variety of target outputs on behaviorally relevant time scales through reward-based training. Motivated by diffuse neuromodulatory innervation of M1[19,23,24], we find that coarse-grained control of neuronal gains achieves a performance similar to that of neuron-specific modulation. We demonstrate that we can combine previously learned modulatory gain patterns to accurately generate new desired movements. Therefore, gain patterns can act as motor primitives for quickly constructing novel movements[25,26]. Finally, we show how to control the speed of an intended movement through gain modulation. We find that it is possible to learn gain patterns that affect either only the shape or only the speed of a movement, thus enabling efficient and independent movement control in space and time.

Results

Modeling gain modulation in recurrent neuronal networks. To understand how cortical networks can efficiently generate a large variety of outputs, we begin with an existing cortical circuit model[11]. We use recurrent networks, with $N=2M$ neurons (with M excitatory and M inhibitory neurons), for which the neuronal activity vector $\boldsymbol{x}(t)=(x_1(t),\ldots,x_N(t))^{\mathrm{T}}$ evolves according to

$$\tau\frac{d\boldsymbol{x}(t)}{dt}=-\boldsymbol{x}(t)+\boldsymbol{W}f(\boldsymbol{x}(t);\boldsymbol{g}), \tag{1}$$

where the single-neuron time constant is $\tau=200$ ms, and (unless we state otherwise) we generate the synaptic weight matrix $\boldsymbol{W}$ in line with ref. [11] (i.e., we use 'stability-optimized circuits'). These networks consist of a set of sparse, strong excitatory weights that are balanced by fine-tuned inhibition (see Methods).

The gain function f, which governs the transformation of neuronal activity $\boldsymbol{x}$ into firing rates relative to a baseline rate r_0, is

$$f(x_i;g_i)=\begin{cases} r_0\tanh(g_ix_i/r_0), & \text{if } x_i<0,\\ (r_{\max}-r_0)\tanh(g_ix_i/(r_{\max}-r_0)), & \text{if } x_i\geq 0,\end{cases} \tag{2}$$

where the gain g_i is the slope of the function f at the baseline rate r_0 and thus controls the input–output sensitivity of neuron i. In equation (1), $f(\boldsymbol{x};\boldsymbol{g})$ denotes the element-wise application of the scalar function f to the neuronal activity vector $\boldsymbol{x}$. Unless we state otherwise, we use a baseline rate of $r_0=20$ Hz and a maximum firing rate

[1]Centre for Neural Circuits and Behaviour, University of Oxford, Oxford, UK. [2]Department of Mathematics, University of California Los Angeles, Los Angeles, CA, USA. [3]Mathematical Institute, University of Oxford, Oxford, UK. [4]CABDyN Complexity Centre, University of Oxford, Oxford, UK. [5]Computational and Biological Learning Lab, Department of Engineering, University of Cambridge, Cambridge, UK. *e-mail: jake.stroud@cncb.ox.ac.uk

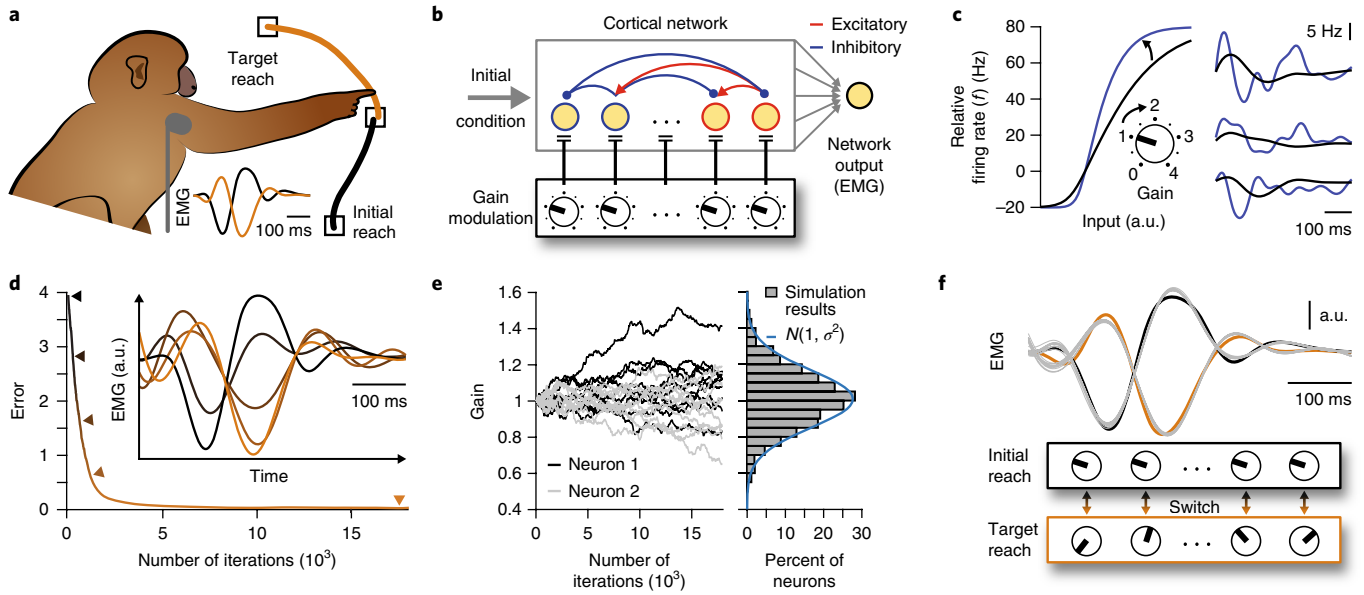

Fig. 1 | Controlling network activity through neuron-specific gain modulation. a, Example of a reaching task, with illustrative electromyograms (EMGs) of muscle activity for two reaches (in orange and black). **b**, Schematic of our model (see the text and Methods). **c**, Changing the slope of the input–output gain function (left) uniformly for all neurons from 1 (black) to 2 (blue) has pronounced effects on neuronal firing rates (right). We show results for three example neurons. **d**, The mean error in network output decreases during training with neuron-specific modulation. Inset: five snapshots of network output (indicated by arrowheads) as learning progresses. (The black curve is the network output with all gains set to 1.) **e**, Left: neuronal gain changes during training for two example neurons (gray and black) and 10 training sessions with the same target. Right: histogram of gain values after training. The blue curve is a Gaussian fit with an s.d. of $\sigma \approx 0.157$. **f**, Network outputs (gray curves) with all gains set to 1 and a new learned gain pattern for 10 noisy initial conditions compared to both targets (black and orange). We use a 200-neuron network for all simulations in this figure.

of $r_{max} = 100$ Hz, consistent with experimental observations[4,27]. The gain function $f(\boldsymbol{x}; \boldsymbol{g})$ describes the neuronal firing rates relative to the baseline steady-state r_0[28]. Identical dynamics can also result from using a strictly positive gain function, combined with a tonic (i.e., static) external input (see Methods).

For appropriate initial conditions $\boldsymbol{x}(t=0) = \boldsymbol{x}_0$ (see Methods), the neuronal dynamics given by equation (1) exhibit naturalistic activity transients that resemble M1 recordings[4,11], and the population activity is rich enough to enable the generation of complex movements through linear readouts[11]. We emulate neuromodulation in this model by directly controlling the input–output gain g_i of each neuron (Fig. 1b,c).

Neuron-specific gain modulation. We find that increasing the gain of all neurons uniformly (i.e., $g_i = g$ in equation (2)) increases both the frequency and amplitude of the neuronal firing rates (Fig. 1c). One can understand these effects of uniform modulation by linearizing equation (1) around $\boldsymbol{x} = \boldsymbol{0}$, yielding the linear ordinary differential equation $\tau \frac{d\boldsymbol{x}}{dt} = (g\boldsymbol{W} - \boldsymbol{I})\boldsymbol{x}$ (where $\boldsymbol{I}$ is the identity matrix), and studying changes in the spectrum of the matrix $g\boldsymbol{W} - \boldsymbol{I}$ (see Supplementary Math Note).

To allow more precise control of neuronal activity than through uniform modulation, we can independently adjust the gain of each neuron in what we call 'neuron-specific modulation'. We obtain gain patterns that lead to the generation of target output activity using a reward-based node-perturbation learning rule (see Methods). Our rule, which acts on the modulatory pathway of our model but is similar to proposed synaptic plasticity rules for reward-based learning[29–32], uses a global scalar signal of recent performance to iteratively adjust each neuron's gain while the initial condition $\boldsymbol{x}_0$ and the network architecture remain fixed.

Starting with a network and readout weights that produce an initial movement with all gains set to 1 (Fig. 1d), our learning rule yields a gain pattern that leads to the successful generation of a novel target movement after a few thousand training iterations (Fig. 1d; and see Methods). Errors between the actual and desired outputs tend to decrease monotonically and eventually become negligible. Independent training sessions with the same target movement produce nonidentical but positively correlated gain patterns (Fig. 1e and Supplementary Fig. 1c). Counterintuitively, the neuronal firing rates change only slightly, even though the network output is altered substantially (Supplementary Fig. 1b). After learning the target, the same initial condition can produce either of two distinct network outputs, depending on the applied gain pattern (Fig. 1f). The outputs are also similarly robust with respect to noisy initial conditions for each gain pattern (Supplementary Fig. 1d).

We also compare the learning performance of gain modulation with alternative learning mechanisms. We train either the neuronal gains, the initial condition $\boldsymbol{x}_0$ of the neuronal activity, a rank-1 perturbation of the synaptic weight matrix, or the full synaptic weight matrix using back-propagation (see Methods). We find empirically for this task that training through gain modulation yields a learning performance similar to that achieved by training the initial condition or the full synaptic weight matrix and that training through gain modulation performs substantially better than learning a rank-1 perturbation of the synaptic weight matrix (Supplementary Fig. 1f).

Gain modulation in different models. We now examine whether learning through gain modulation is possible in alternative, commonly used variants of our model. Motor circuits that drive movements also engage in periods of movement preparation[5,7,33], suggesting a role for gain modulation in shaping circuit dynamics during both movement planning and movement execution. We find that learning is also possible in a model in which we include gain modulation during movement planning. We simulate the preparatory period using a ramping input to the system[11] (see Methods),

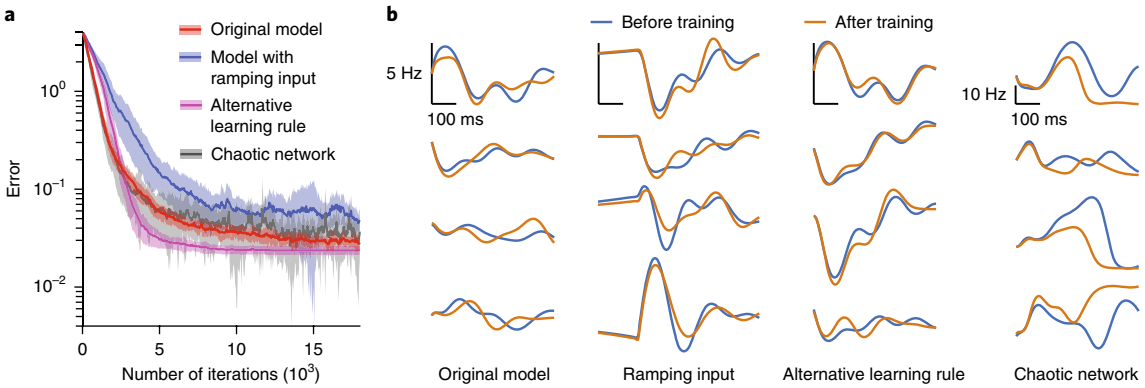

Fig. 2 | Learning through gain modulation in different models. a, Mean error over 10 independent training sessions for our original model from Fig. 1d (red); the model with a biologically motivated ramping input (blue); the model when using the alternative learning rule equation (10), in which learning automatically stops at a sufficiently small error (purple); and when using a 'chaotic' recurrent network model (gray; see Methods). Shading indicates one s.d. **b**, The firing rates of four example neurons before (i.e., with all gains set to 1) and after training the neuronal gains in (left) our original model, (center left) our model with a ramping input, (center right) our model with the alternative learning rule, and (right) the model when using a chaotic network. We use 200-neuron networks for all simulations in this figure.

such that gain modulation now directly affects the neuronal activity at movement onset. We find that learning performance (i.e., error reduction) for the task that we show in Fig. 1d is slightly poorer if we employ a ramping input than if we do not (Fig. 2a). This occurs because gain modulation during the preparatory phase changes the neuronal activity at movement onset, allowing it to leave the null space of the readout weights (which are fixed) and thus elicit premature muscle activity at movement onset.

We also construct a 'chaotic' variant of our model[34] (see Methods) for the same task and train only the neuronal gains. We achieve learning performance (Fig. 2a) similar to that achieved by our original model in Fig. 1d, even though the neuronal firing rates are very different (Fig. 2b). Finally, we also use an alternative learning rule to train the neuronal gains (see equations (10) and (11)); in this rule, learning slows down as the decrease in error slows down (see Methods). We find that the error decreases at a faster rate than that in our original learning rule (Fig. 2a). This may occur because the variance of the noise perturbation term in the alternative learning rule becomes smaller over training iterations as the error decreases. Notably, in all of these examples, changes in neuronal responsiveness alone—for example, via inputs from neuromodulatory afferents—can cause dramatic changes in network outputs, thereby providing an efficient mechanism for rapid switching between movements, without requiring any changes in either synaptic architecture or the initial condition $\boldsymbol{x}_0$.

Coarse, group-based gain modulation. Individually modulating the gain of every neuron in motor cortex is likely unrealistic. In line with the existence of diffuse (i.e., not neuron-specific) neuromodulatory projections to M1[19,23,24], we cluster neurons into groups so that we identically modulate units within a group (Fig. 3a; and see Methods). We find that such coarse-grained modulation gives performance similar to that of neuron-specific control for as few as 20 randomly formed groups (see Methods) using our 200-neuron network model from Fig. 1 (Fig. 3b and Supplementary Fig. 2a). For a given number of groups, we can improve performance if, instead of grouping neurons randomly as above, we use a specialized clustering for each movement that is based on previous training sessions (Fig. 3b and Supplementary Fig. 2a; and see Methods). Notably, there exist specialized groupings that perform similarly across multiple different movements (Fig. 3c and Supplementary Fig. 2b,c). Such specialized groupings acquired from learning one set of movements also perform well on novel movements (Supplementary Fig. 2d).

Notably, even with random groupings, network size hardly affects learning performance for a single readout (Fig. 3d). Performance depends much more on the number of groups than on the number of neurons per group. When the task involves two or more readout units, larger networks do learn better, and achieving a good performance necessitates using a larger number of independently modulated groups (Fig. 3e,f). Finally, smaller networks typically learn faster (Fig. 3e), but they ultimately exhibit poorer performance, demonstrating that there is a trade-off between network size, number of groups, and task complexity (i.e., the number of readout units).

Gain patterns can provide motor primitives for novel movements. In principle, it is possible to independently learn numerous gain patterns, supporting the possibility of a repertoire (which we call a 'library') of modulation states that a network can use, in combination, to produce a large variety of outputs. Generating new movements is much more efficient if it is possible to 'intuit' new gain patterns as combinations of previously acquired primitives[15,26]. To test whether this is possible in our model, we first approximate a novel target movement as a convex combination of existing movements (we call this a 'fit' in Fig. 4; see Methods). We then use the same combination of the associated library of gain patterns to construct a new gain pattern (Fig. 4a). Notably, the resulting network output closely resembles the target movement (Fig. 4b). This may seem unintuitive, but one can understand this result mathematically by calculating power-series expansions of the solution of the linearized neuronal dynamics (see Supplementary Math Note).

Finally, increasing the number of elements in the movement library reduces the error between a target movement and its fit, which is also reflected in a progressively better match between the target and the network output (Fig. 4b–d and Supplementary Fig. 3). Although the idea of using motor primitives to facilitate rapid acquisition of new movements is well-established[25,26], our approach proposes the first (to our knowledge) circuit-level mechanism for achieving this objective. In addition to neuromodulatory systems[19,20,22], the cerebellum is a natural candidate structure to coordinate such motor primitives[25], as it is known to project to M1 and to play a critical role in error-based motor learning[25,35].

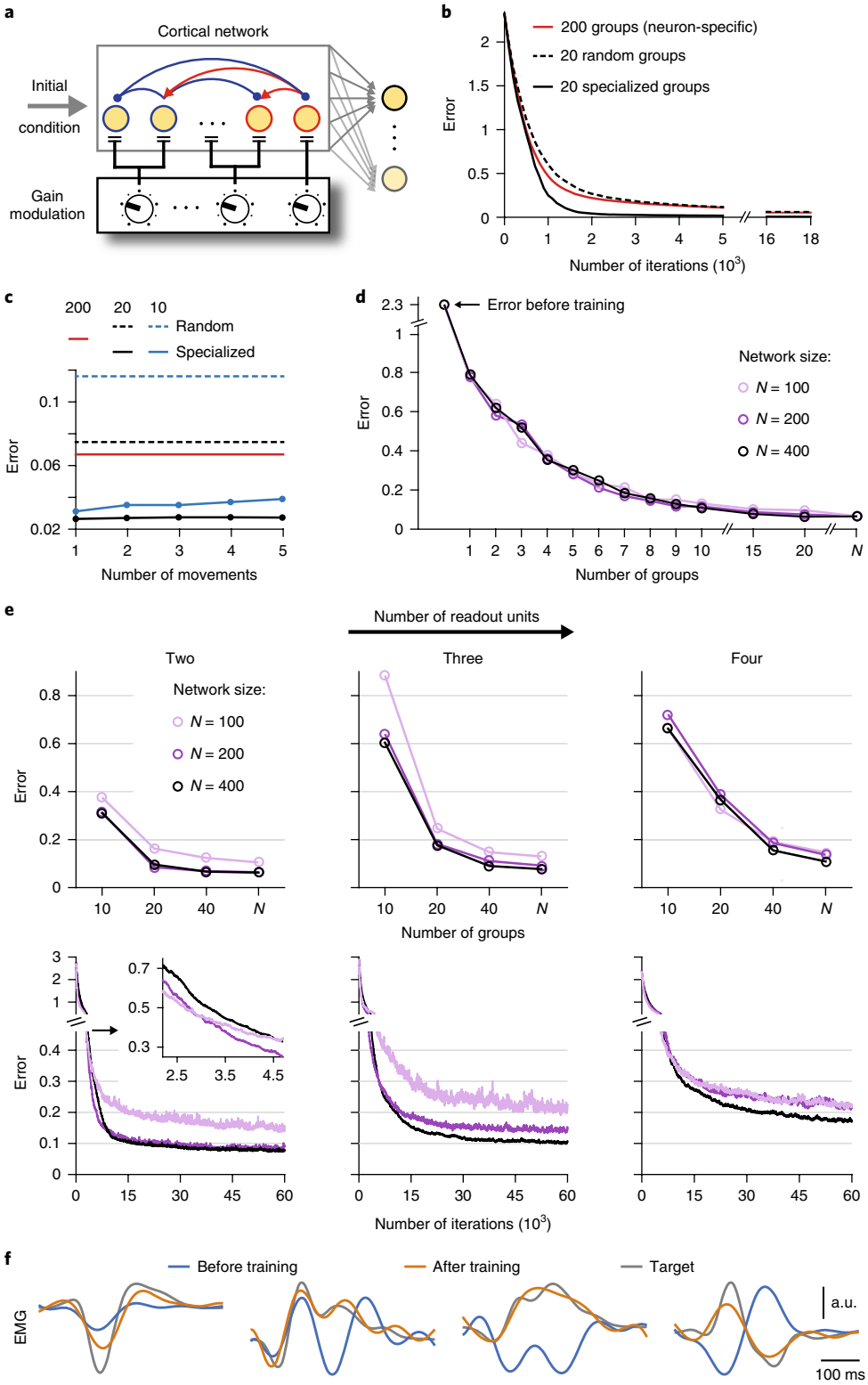

Fig. 3 | Controlling network activity through coarse, group-based gain modulation. a, We identically modulate neurons within each group (see Methods). Target outputs can involve multiple readout units. **b**, Mean error during training for 20 random, 20 specialized, and 200 (i.e., neuron-specific) groups. (See Methods for more details.) **c**, Mean minimum errors after training using specialized groups. We use the same grouping for learning multiple different movements. In **b**,**c**, we use a 200-neuron network. **d**, Mean minimum errors for different numbers of random groups with networks of 100, 200, and 400 neurons. (The *N* on the horizontal axis indicates neuron-specific modulation.) In **b**–**d**, we use a single readout unit. **e**, Top: mean minimum error as a function of the number of random groups when learning each of (left) two, (center) three, and (right) four readouts for the same networks as in **d**. Bottom: the corresponding mean errors during training for the case of 40 groups. The inset is a magnification of the initial training period for the case of two readout units. **f**, Outputs producing the median error for the case of four readout units using 40 groups in the 400-neuron network.

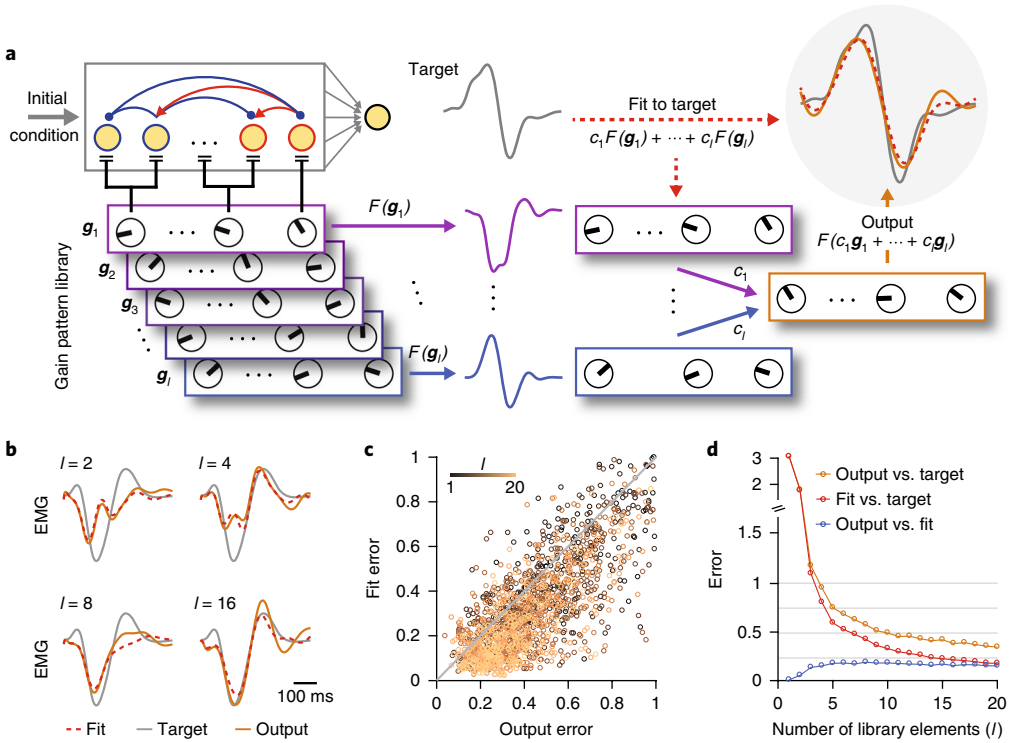

Fig. 4 | Gain patterns can provide motor primitives for novel movements. a, Schematic of a learned library of gain patterns ($\boldsymbol{g}_1$, …, $\boldsymbol{g}_l$, which we color from purple to blue) and a combination $c_1F(\boldsymbol{g}_1) + \ldots + c_lF(\boldsymbol{g}_l)$ of their outputs (which we denote by F) that we fit (red dashed curve) to a novel target (gray curve). Top right: the output $F(c_1\boldsymbol{g}_1 + \ldots + c_l\boldsymbol{g}_l)$ (orange) of the same combination of corresponding gain patterns also closely resembles the target. We use a 400-neuron network with 40 random modulatory groups (see Methods). **b**, Example target, fit, and output (gray, red dashed, and orange curves, respectively) producing the 50th-smallest output error over 100 randomly generated combinations (see Methods) of l library elements using $l = 2$, $l = 4$, $l = 8$, and $l = 16$. **c**, Fit error vs. output error for 100 randomly generated combinations of l library elements for $l = 1, \ldots, 20$. We show the identity line in gray. Each point represents the 50th-smallest error between the output and the fit across 100 novel target movements. **d**, Median errors of the 100 randomly generated combinations of l library elements vs. the number of library elements.

Nonlinear behavior. We initially choose the baseline firing rate ($r_0 = 20$ Hz in equation (2)) to be consistent with experimentally measured firing rates in motor cortex[4,27,36]. Most of the time, neurons operate within the linear part of their nonlinear gain function. In other words, the neuronal dynamics resemble those when using the linear gain function $f(x_i; g_i) = g_ix_i$ (Fig. 5a,c). To test whether our results hold for scenarios with more strongly nonlinear dynamics, we reduce the baseline firing rate to $r_0 = 5$ Hz. This increases the neuronal activity near the lower-saturation regime (i.e., towards the left part of the curve in the left panel of Fig. 1c) of the gain function (Fig. 5b,c). As expected from the larger range of possible network outputs (and improved learning performance) in nonlinear recurrent neuronal networks than in linear ones[31,32,34], we observe better learning performance for $r_0 = 5$ Hz than for $r_0 = 20$ Hz (Fig. 5d); and we obtain a very similar distribution of gain values after training (Fig. 5e).

Notably, it is still possible to learn new movements by using combinations of existing gain patterns. As before, performance is limited by the accuracy with which one can construct target movements as linear combinations of existing primitives (Supplementary Fig. 4b). Moreover, errors in network output decrease, on average, with increasing numbers of gain patterns in the movement library (Fig. 5f), and the difference between the network output and corresponding fit remains small for all tested numbers of library elements (Fig. 5f). However, reducing r_0 to sufficiently small values ($r_0 < 5$ Hz) does eventually lead to a deterioration in the effectiveness of gain patterns at providing motor primitives for new movements.

Gain modulation can control movement speed. Thus far, we have demonstrated that simple (even coarse, group-based) gain modulation enables control of network outputs of the same fixed duration. To control movements of different durations, motor networks must be able to slow down or speed up muscle outputs (i.e., change the duration of movements without affecting their shape). In line with recent experimental results[37,38], we investigate whether changing neuronal gains allows control of the speed of an intended movement (Fig. 6a; and see Methods). We begin with a network of 400 neurons (with 40 random modulatory groups) that generates muscle activity lasting approximately 0.5 s. We find that our learning rule can successfully train a network to generate a slower variant that lasts five times longer (Fig. 6b and Supplementary Fig. 5a) than the original movement (see Methods).

In contrast to simply changing the single-neuron time constant τ—which uniformly scales the duration, but does not affect the shape of each neuron's activity—modifying neuronal gains to generate 'fast' and 'slow' output variants leads to changes in both the shape and duration of neuronal firing rates, in line with recent experimental findings[37]. Changing neuronal gains thus enables interactions between the shape and duration of outputs without requiring retraining of the synaptic weight matrix to scale the duration of neuronal activities[39].

The learned slow variants are more sensitive to noisy initial conditions than the fast variants, but we can find more robust solutions by using a regularized back-propagation algorithm to train both the neuronal gains and the readout weights (see Methods). Following such training, the network successfully learns the slow variants

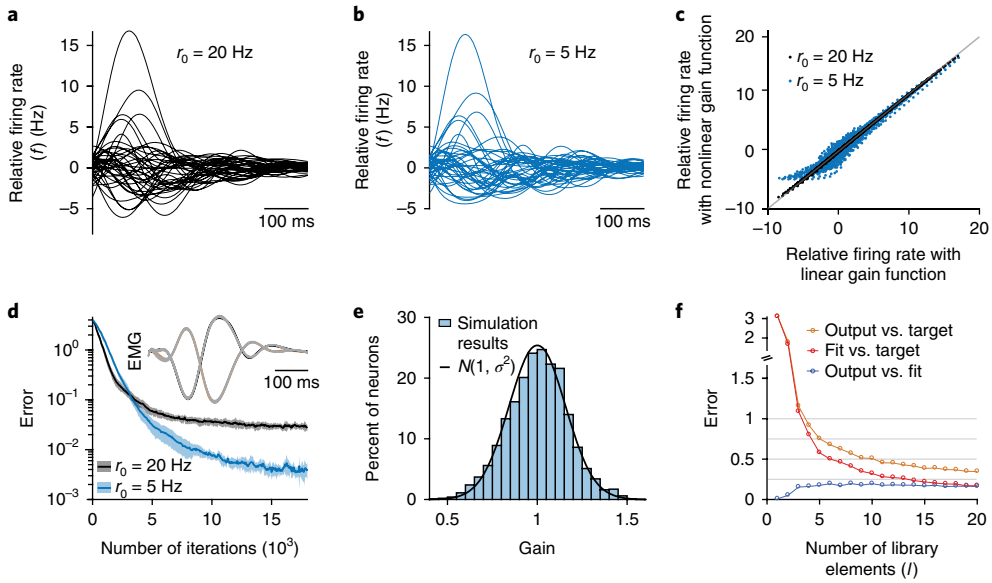

Fig. 5 | Examining effects of more strongly nonlinear neuronal dynamics by using a baseline rate of $r_0 = 5$ Hz. a, Relative firing rate of 20 excitatory and 20 inhibitory neurons in a 200-neuron network with $r_0 = 20$ Hz in equation (2). **b**, Relative firing rate of the same neurons as those in **a**, but with $r_0 = 5$ Hz. **c**, The dotted curves show the relative firing rates of all neurons over time when using the nonlinear gain function (see equation (2)) with (black) $r_0 = 20$ Hz and (blue) $r_0 = 5$ Hz vs. the relative firing rates that result from using the linear gain function $f(x_i; g_i) = g_i x_i$. We set each neuronal gain g_i to 1, and we plot the identity line in gray. **d**, Mean error over 10 independent training sessions with $r_0 = 20$ Hz (black) and $r_0 = 5$ Hz (blue) for the task in Fig. 1d (see Methods). Shading indicates 1 s.d. Inset: network outputs with all gains set to 1 and the new learned gain pattern with $r_0 = 5$ Hz for 10 noisy initial conditions (gray curves). We show the two targets in black and orange (see Methods). **e**, Histogram of gain values after training with $r_0 = 5$ Hz. The black curve is a Gaussian distribution with a mean of 1 and an s.d. of $\sigma \approx 0.157$ (i.e., the distribution that we obtained with $r_0 = 20$ Hz in Fig. 1e). **f**, Gain patterns as motor primitives with $r_0 = 5$ Hz. We generate these results as in Fig. 4d, except that now we use $r_0 = 5$ Hz. We obtain qualitatively similar results to our observations for the baseline rate $r_0 = 20$ Hz.

(Fig. 6c), which are now less sensitive to the same noisy initial conditions (Supplementary Fig. 5g). The neuronal dynamics oscillate transiently, with a substantially lower frequency than either the fast variants or the slow variants trained by our reward-based learning rule (Fig. 6b,c). We also find a single gain pattern that, rather than slowing down only one movement, can slow down up to approximately five distinct movements (which result from five orthogonal initial conditions) by a factor of 5 (Supplementary Fig. 5h–j). Consequently, one can extend the temporal scale of transient neuronal activity several-fold through specific changes in neuronal gains.

Smoothly controlling the speed of movements. Following training on a fast and a slow variant of the same movement (see the previous section), we find that naively interpolating between the two gain patterns does not yield the same movement at intermediate speeds (Fig. 6d), consistent with human subjects being unable to consistently apply learned movements at novel speeds[39,40]. Therefore, even when we consider fast and slow variants of the same movement, both our learning rule and the back-propagation training do not learn to 'slow down' the movement; instead, they learn two seemingly unrelated gain patterns. However, it is possible to modify our back-propagation training procedure by including additional constraints on the fast and slow gain patterns (see Methods) so that interpolating between the two gain patterns produces progressively faster or slower outputs. We successfully train the network to generate two movements (associated with two different initial conditions) at seven different speeds with durations ranging from 0.5 s to 2.5 s (Fig. 6e and Supplementary Fig. 6; and see Methods). Linear interpolation between the fast and slow gain patterns (Supplementary Fig. 6b) now generates smooth speed control of both movements at any intermediate speed (Fig. 6d,f). In other words, we can control the speed of multiple movements associated with different initial conditions by learning a 'manifold'[41] in neuronal gain space that interpolates between the fast and the slow gain patterns (Fig. 6a).

Joint control of movement shape and speed. Thus far, we have shown that gain modulation can affect either the shape or the speed of a movement. Flexible and independent control of both the shape and speed of a movement (i.e., joint control) necessitates separate representations of space and time in the gain patterns. A relatively simple possibility is to find a single universal manifold in neuronal gain space (see the previous section) for speed control (we call this the 'speed manifold') and combine it with gain patterns that are associated with different movement shapes. Biologically, this may be achievable using separate modulatory systems. We achieve such separation by simultaneously training one speed manifold and ten gain patterns for ten different movement shapes, such that movements are encoded by the product of shape-specific and speed-specific gain patterns (Fig. 7a; and see Methods). Following training, we can generate each of the ten movements at the seven trained speeds by multiplying a speed-specific gain pattern (Fig. 7b) with the desired shape-specific gain pattern. Critically, we can also accurately generate each of the ten different movements at any intermediate speed by simply linearly interpolating between the fast and slow gain patterns (Fig. 7c,d). We thereby obtain separate families of gain patterns for movement shape and speed that independently control movements in space and time.

Learning gain-pattern primitives to control movement shape and speed. To construct new movement shapes with arbitrary durations, we examine the possibility of using both the speed manifold and the ten trained shape-specific gain patterns that we obtained previously (Fig. 7) as a library of spatiotemporal motor primitives. We test this library using 100 novel target movement shapes (as we did in Fig. 4).

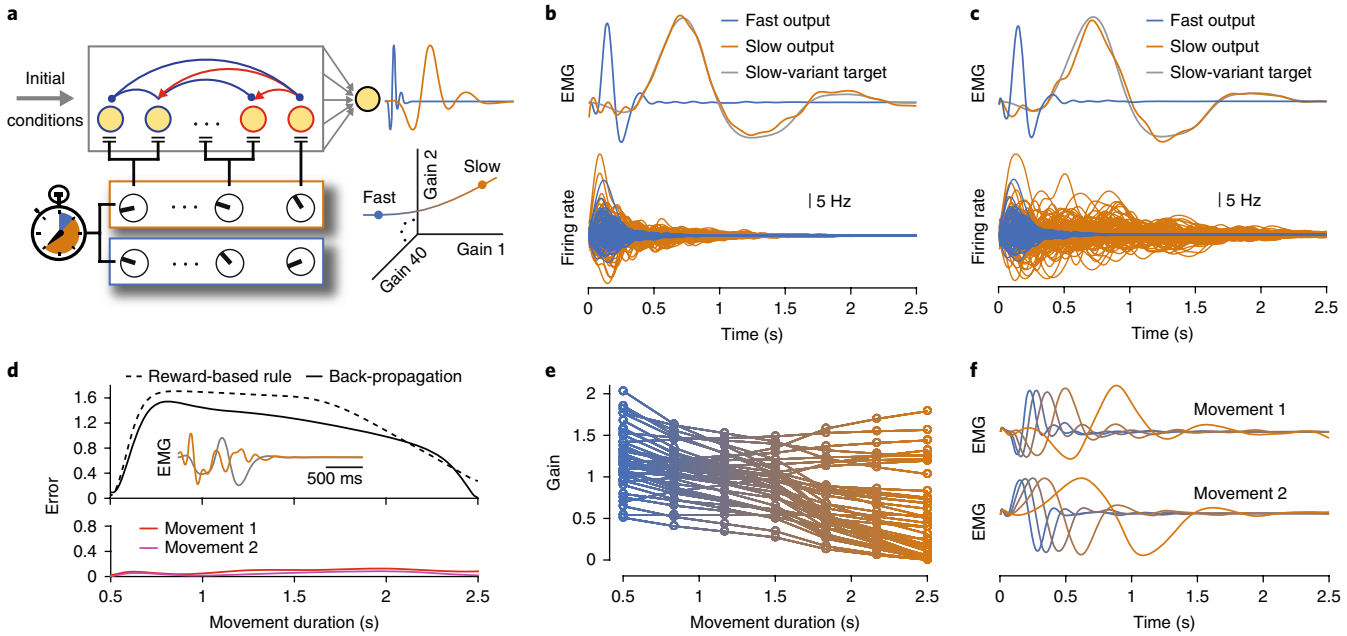

Fig. 6 | Gain modulation can control movement speed. a, Schematic of gain patterns for fast (0.5 s; blue) and slow (2.5 s; orange) movement variants. Bottom right: illustration of a manifold in neuronal gain space for controlling movement speed (see the text). We train a 400-neuron network using 40 random modulatory groups for all simulations (see Methods). **b**, Top: we train a network to extend its output from a fast-movement to a slow-movement variant using our reward-based learning rule. Bottom: example firing rates of 50 excitatory and 50 inhibitory neurons for both fast and slow speed variants. **c**, As in **b**, but now we use a back-propagation algorithm to train the neuronal gains (see Methods). **d**, Top: interpolation between fast and slow gain patterns does not reliably generate target outputs of intermediate speeds when trained only at the fast and slow speeds. We show an example output (orange) that lasts 1.5 s and the associated target (gray). Bottom: linear interpolation between the fast and slow gain patterns successfully generates target outputs when trained at five intermediate speeds. We train one set of gain patterns (see **e**) on two target outputs associated with two different initial conditions (see Methods). **e**, The seven optimized gain patterns for all 40 modulatory groups when training at seven evenly spaced speeds. **f**, Both outputs when linearly interpolating at five evenly spaced speeds between the fast and slow gain patterns from **e.**

For each target movement, we learn the coefficients for linearly combining the ten shape-specific gain-pattern primitives to obtain each new movement at both the fast and slow speeds, while keeping the speed manifold fixed (Fig. 8a; and see Methods).

We find that it is possible to accurately generate the new movements at fast and slow speeds using the above spatiotemporal library of gain patterns (Supplementary Fig. 7). Critically, we are able to produce the new movements with accuracies similar to those at the fast and slow speeds at any intermediate speed by linearly interpolating between the fast and slow gain patterns using the unaltered speed manifold (Fig. 8b,c). The mean error of approximately 0.5 across all movement durations is similar to the error that we obtained previously from a movement library consisting of ten gain patterns (Fig. 4d). We can substantially outperform the (uniformly at random) permuted gain patterns from their associated targets and outputs generated using least-squares fitting (which we used in Fig. 4) to combine gain patterns (Fig. 8c; and see Methods).

Consistent with the idea of rapidly generating movements using motor primitives, we generate correlated target shapes by using correlated combinations of gain patterns (Fig. 8d). Therefore, one can use previously learned gain patterns for controlling movement shapes to generate new movements while maintaining independent control of movement speed.

Discussion

The movement-specific population activity that has been observed in monkey primary motor cortex[4] can arise through several possible mechanisms. Distinct neuronal activity can emerge from a fixed population-level dynamical system with different movement-specific preparatory states[7]. Alternatively, one can change the underlying dynamical system through modification of the effective connectivity[42], even when a preparatory state is the same across movements. Such changes in effective connectivity can arise either through a feedback loop (for example, a low-rank addition to the synaptic weight matrix[34]) or through patterns of movement-specific gains, as we explore in this paper. We find that movement-specific gain patterns provide a performance level similar to that achieved by training a different initial condition for each desired output (with a fixed duration) and that both of these approaches outperform a rank-1 perturbation of the synaptic weight matrix (see Supplementary Fig. 1f). Gain modulation thus provides a complementary method of controlling neuronal dynamics for flexible and independent manipulation of output shape. Additionally, gain modulation provides a compelling mechanism for extending the duration of activity transients without needing to carefully construct movement-specific network architectures[39].

Gain modulation may occur via neuromodulators[20,22], but it can also arise from a tonic (i.e., static) input that shifts each neuron's resting activity within the dynamic range of its input–output function (for example, through inputs from the cerebellum)[14]. Although this is an effective way of mimicking gain changes in recurrent network models with strongly nonlinear single-neuron dynamics[37,43], we are unable to produce desired target outputs by training a tonic input. It is worth noting that a tonic input also modifies baseline neuronal activity, thereby altering the output muscle activities away from rest.

In line with previous research[4,8,10], we train networks to generate specific target output trajectories (which we suggest act as a proxy for muscle activity). This is a simplification of actual motor learning, as there are many different possible muscle activations that can

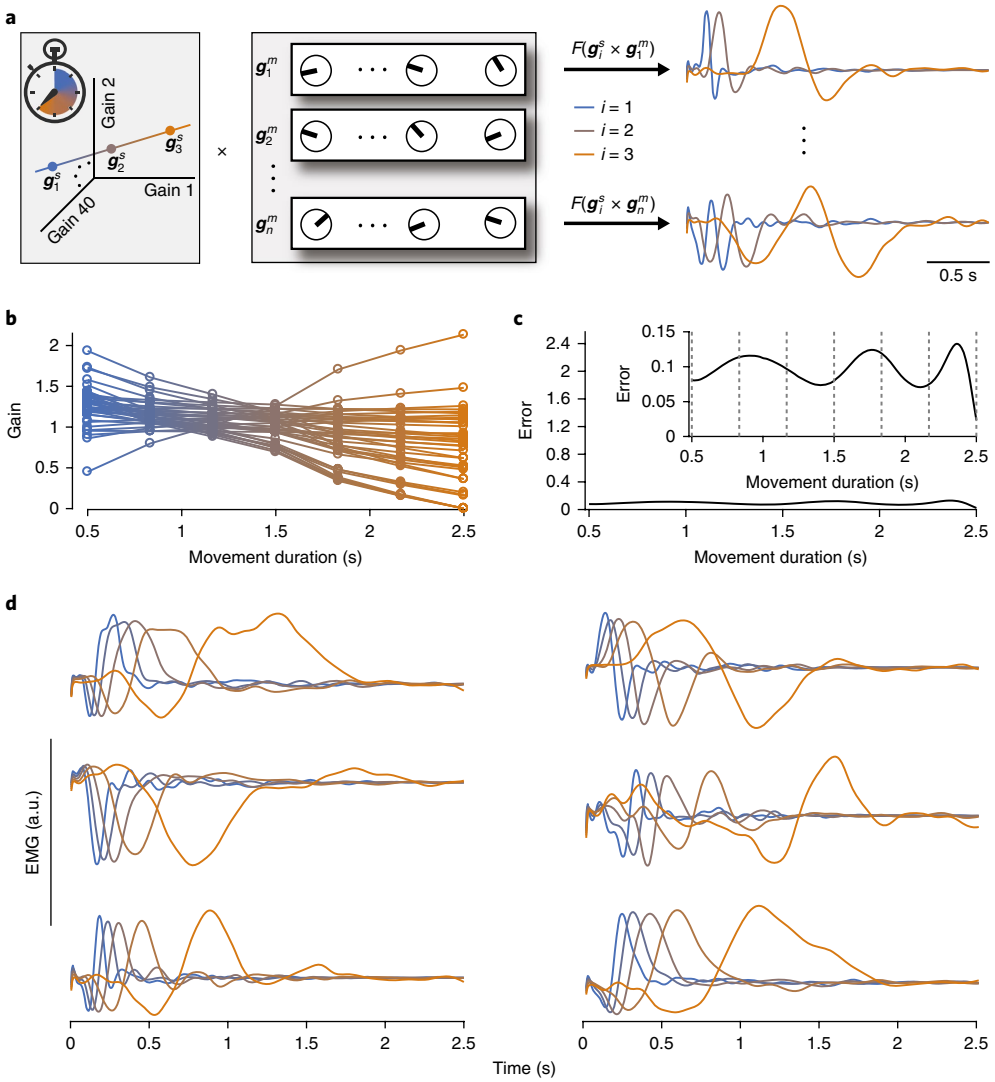

Fig. 7 | Joint control of movement shape and speed through gain modulation. a, One can jointly learn the gain patterns g_i^s for (left) movement speed and g_j^m for (center) movement shape so that the product of two such gain patterns produces a desired movement at a desired speed. Right: example outputs (which we denote by *F*) for two movement shapes at three interpolated speeds between the fast and slow gain patterns (see the main text and Methods). **b**, Seven optimized gain patterns for controlling movement speed (i.e., g_i^s for $i \in \{1, \ldots, 7\}$ from **a**) for the 40 modulatory groups when training on 10 different movement shapes. **c**, We plot the mean error over all 10 movements when linearly interpolating between the fast and slow gain patterns for controlling movement speed from **b**. Vertical axis scale is as in Fig. 6d. Inset: we plot the same data using a different vertical axis scale. Vertical dashed lines identify the seven movement durations that we use for training. **d**, Outputs at five interpolated speeds between the fast and slow gain patterns for six of the ten movements. For each simulation, we train a 400-neuron network using 40 random modulatory groups (see Methods).

lead to a 'successful' movement. For some motor tasks, it is probably more biologically plausible to train a network to increase the success of a desired movement defined by the position of an end effector while also minimizing the total amount of muscle activity (for example, see refs [32,44]). Nevertheless, our learning rule is biologically plausible, in that it uses only local information and a single scalar signal (which is the total sum of squared errors) per trial. It does not carry detailed information about the exact way in which an output trajectory deviates from a desired trajectory. We thus expect that our main results will still be relevant for more realistic models of motor learning (for example, using a biophysically realistic model of a human arm[32]).

In our model, in which the recurrent architecture remains fixed, synaptic modifications may take place upstream of the motor circuit (for example, in the input synapses to the presumed neuromodulatory neurons[45]). Additionally, changes in neuronal gains can work in concert with synaptic plasticity in cortical circuits, thereby allowing changes in the modulatory state of a network to be transferred into circuit connectivity[46], consistent with known interactions between neuromodulation and plasticity[45]. Consequently, understanding the neural basis of motor learning may necessitate recording from a potentially broader set of brain areas than those circuits whose activity correlates directly with movement dynamics.

Our results build on a growing literature of taking a dynamical-systems approach to studying temporally structured cortical activity. This perspective has been effective for investigations of several cortical regions[4,5,7,36,37,47,48]. In line with this approach, our results may also be applicable to other recurrent cortical circuits that exhibit rich temporal dynamics (for example, decision-making dynamics in prefrontal cortex[48], temporally structured memories, etc.).

In summary, our results support the view that knowing only the structure of neuronal networks is not sufficient to explain their dynamics[49,50]. We extend current understanding of the effects of neuromodulation[13,17,20,49] and show that it is possible to control a

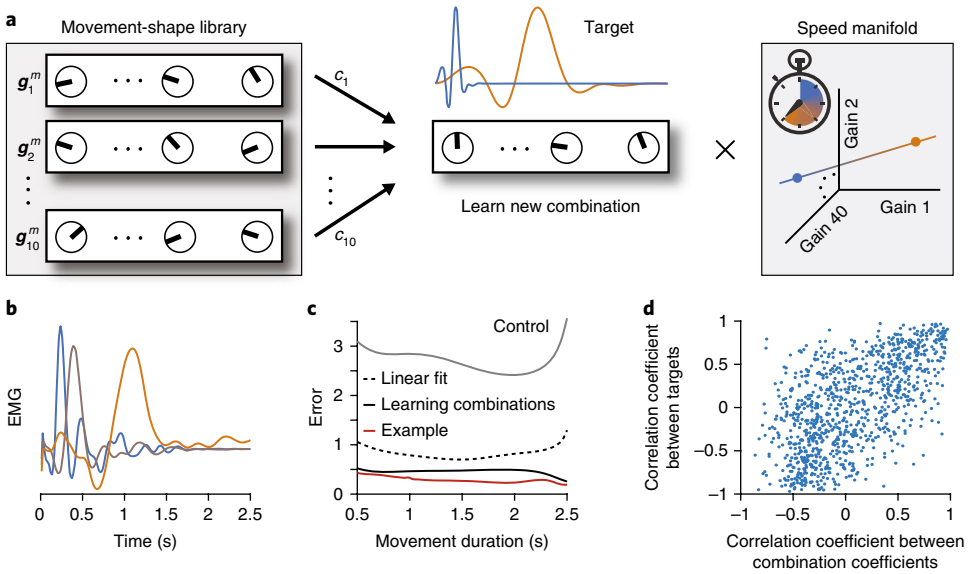

Fig. 8 | Learning gain-pattern primitives to control movement shape and speed. a, We are able to learn to combine (left) previously acquired gain patterns for movement shapes to generate (center) a new target movement at both fast and slow speeds simultaneously using (right) a fixed manifold in neuronal gain space for controlling movement speed (see Methods). **b**, We plot the output, at three different speeds, that produces the 50th-smallest error (across all 100 target movements) between the output and the target when summing errors at both fast and slow speeds. **c**, Mean network output error across all 100 target movements for all durations when learning to combine gain patterns (black solid curve). The red curve indicates the error for the output from **b**. As a control, we plot the mean error over all target movements when dissociating the learned gain patterns from their target movement by permuting (uniformly at random) the target movements (gray curve). We also plot the mean error over all target movements when combining gain patterns using a least-squares fit of the ten learned movement shapes to the target (black dashed curve; see Methods). For each example, to generate outputs of a specific duration, we linearly interpolate between the fast and slow gain patterns. **d**, We plot the Pearson correlation coefficient between each pair of target movements vs. the Pearson correlation coefficient between the corresponding pair of learned combination coefficients c_1, …, c_{10}. For each simulation, we train a 400-neuron network using 40 random modulatory groups (see Methods).

recurrent neuronal network's computations without changing its connectivity. We find that modulating only neuronal responsiveness enables flexible control of neuronal activity. We are also able to combine previously learned modulation states to generate new desired activity patterns, and we demonstrate that employing gain modulation allows one to smoothly and accurately control the duration of network outputs. Our results thus suggest the possibility that gain modulation is a central part of motor control.

Online content

Any methods, additional references, Nature Research reporting summaries, source data, statements of data availability, and associated accession codes are available at https://doi.org/10.1038/s41593-018-0276-0.

Received: 15 May 2018; Accepted: 9 October 2018;
Published online: 26 November 2018

References

1. Rathelot, J.-A. & Strick, P. L. Subdivisions of primary motor cortex based on cortico-motoneuronal cells. *Proc. Natl. Acad. Sci. USA* **106**, 918–923 (2009).
2. Rosenbaum, D. A. *Human Motor Control*. (Academic Press, Cambridge, MA,USA, 2009).
3. Sanes, J. N. & Donoghue, J. P. Plasticity and primary motor cortex. *Annu. Rev. Neurosci.* **23**, 393–415 (2000).
4. Churchland, M. M. et al. Neural population dynamics during reaching. *Nature* **487**, 51–56 (2012).
5. Shenoy, K. V., Sahani, M. & Churchland, M. M. Cortical control of arm movements: a dynamical systems perspective. *Annu. Rev. Neurosci.* **36**, 337–359 (2013).
6. Afshar, A. et al. Single-trial neural correlates of arm movement preparation. *Neuron* **71**, 555–564 (2011).
7. Churchland, M. M., Cunningham, J. P., Kaufman, M. T., Ryu, S. I. & Shenoy, K. V. Cortical preparatory activity: representation of movement or first cog in a dynamical machine? *Neuron* **68**, 387–400 (2010).
8. Russo, A. A. et al. Motor cortex embeds muscle-like commands in an untangled population response. *Neuron* **97**, 953–966.e8 (2018).
9. Churchland, M. M. & Cunningham, J. P. A dynamical basis set for generating reaches. *Cold Spring Harb. Symp. Quant. Biol.* **79**, 67–80 (2014).
10. Sussillo, D., Churchland, M. M., Kaufman, M. T. & Shenoy, K. V. A neural network that finds a naturalistic solution for the production of muscle activity. *Nat. Neurosci.* **18**, 1025–1033 (2015).
11. Hennequin, G., Vogels, T. P. & Gerstner, W. Optimal control of transient dynamics in balanced networks supports generation of complex movements. *Neuron* **82**, 1394–1406 (2014).
12. Sehgal, M., Song, C., Ehlers, V. L. & Moyer, J. R. Jr. Learning to learn - intrinsic plasticity as a metaplasticity mechanism for memory formation. *Neurobiol. Learn. Mem.* **105**, 186–199 (2013).
13. Kida, H. & Mitsushima, D. Mechanisms of motor learning mediated by synaptic plasticity in rat primary motor cortex. *Neurosci. Res.* **128**, 14–18 (2018).
14. Chance, F. S., Abbott, L. F. & Reyes, A. D. Gain modulation from background synaptic input. *Neuron* **35**, 773–782 (2002).
15. Swinehart, C. D., Bouchard, K., Partensky, P. & Abbott, L. F. Control of network activity through neuronal response modulation. *Neurocomputing* **58–60**, 327–335 (2004).
16. Zhang, J. & Abbott, L. F. Gain modulation of recurrent networks. *Neurocomputing* **32–33**, 623–628 (2000).
17. Marder, E. Neuromodulation of neuronal circuits: back to the future. *Neuron* **76**, 1–11 (2012).
18. Salinas, E. & Thier, P. Gain modulation: a major computational principle of the central nervous system. *Neuron* **27**, 15–21 (2000).
19. Molina-Luna, K. et al. Dopamine in motor cortex is necessary for skill learning and synaptic plasticity. *PLoS One* **4**, e7082 (2009).
20. Thurley, K., Senn, W. & Lüscher, H.-R. Dopamine increases the gain of the input-output response of rat prefrontal pyramidal neurons. *J. Neurophysiol.* **99**, 2985–2997 (2008).
21. Vestergaard, M. & Berg, R. W. Divisive gain modulation of motoneurons by inhibition optimizes muscular control. *J. Neurosci.* **35**, 3711–3723 (2015).

22. Wei, K. et al. Serotonin affects movement gain control in the spinal cord. *J. Neurosci.* **34**, 12690–12700 (2014).
23. Hosp, J. A., Pekanovic, A., Rioult-Pedotti, M. S. & Luft, A. R. Dopaminergic projections from midbrain to primary motor cortex mediate motor skill learning. *J. Neurosci.* **31**, 2481–2487 (2011).
24. Huntley, G. W., Morrison, J. H., Prikhozhan, A. & Sealfon, S. C. Localization of multiple dopamine receptor subtype mRNAs in human and monkey motor cortex and striatum. *Brain Res. Mol. Brain Res.* **15**, 181–188 (1992).
25. Thoroughman, K. A. & Shadmehr, R. Learning of action through adaptive combination of motor primitives. *Nature* **407**, 742–747 (2000).
26. Giszter, S. F. Motor primitives–new data and future questions. *Curr. Opin. Neurobiol.* **33**, 156–165 (2015).
27. Lara, A. H., Cunningham, J. P. & Churchland, M. M. Different population dynamics in the supplementary motor area and motor cortex during reaching. *Nat. Commun.* **9**, 2754 (2018).
28. Rajan, K., Abbott, L. F. & Sompolinsky, H. Stimulus-dependent suppression of chaos in recurrent neural networks. *Phys. Rev. E* **82**, 011903 (2010).
29. Mazzoni, P., Andersen, R. A. & Jordan, M. I. A more biologically plausible learning rule for neural networks. *Proc. Natl. Acad. Sci. USA* **88**, 4433–4437 (1991).
30. Legenstein, R., Chase, S. M., Schwartz, A. B. & Maass, W. A reward-modulated hebbian learning rule can explain experimentally observed network reorganization in a brain control task. *J. Neurosci.* **30**, 8400–8410 (2010).
31. Hoerzer, G. M., Legenstein, R. & Maass, W. Emergence of complex computational structures from chaotic neural networks through reward-modulated Hebbian learning. *Cereb. Cortex* **24**, 677–690 (2014).
32. Miconi, T. Biologically plausible learning in recurrent neural networks reproduces neural dynamics observed during cognitive tasks. *eLife* **6**, e20899 (2017).
33. Li, N., Chen, T.-W., Guo, Z. V., Gerfen, C. R. & Svoboda, K. A motor cortex circuit for motor planning and movement. *Nature* **519**, 51–56 (2015).
34. Sussillo, D. & Abbott, L. F. Generating coherent patterns of activity from chaotic neural networks. *Neuron* **63**, 544–557 (2009).
35. Spampinato, D. A., Block, H. J. & Celnik, P. A. Cerebellar–M1 connectivity changes associated with motor learning are somatotopic specific. *J. Neurosci.* **37**, 2377–2386 (2017).
36. Kao, J. C. et al. Single-trial dynamics of motor cortex and their applications to brain-machine interfaces. *Nat. Commun.* **6**, 7759 (2015).
37. Wang, J., Narain, D., Hosseini, E. A. & Jazayeri, M. Flexible timing by temporal scaling of cortical responses. *Nat. Neurosci.* **21**, 102–110 (2018).
38. Soares, S., Atallah, B. V. & Paton, J. J. Midbrain dopamine neurons control judgment of time. *Science* **354**, 1273–1277 (2016).
39. Hardy, N. F., Goudar, V., Romero-Sosa, J. L. & Buonomano, D. V. A model of temporal scaling correctly predicts that motor timing improves with speed. *Nat. Commun.* **9**, 4732 (2018).
40. Collier, G. L. & Wright, C. E. Temporal rescaling of simple and complex ratios in rhythmic tapping. *J. Exp. Psychol. Hum. Percept. Perform.* **21**, 602–627 (1995).
41. Gallego, J. A., Perich, M. G., Miller, L. E. & Solla, S. A. Neural manifolds for the control of movement. *Neuron* **94**, 978–984 (2017).
42. Friston, K. J. Functional and effective connectivity: a review. *Brain Connect.* **1**, 13–36 (2011).
43. Sussillo, D. & Barak, O. Opening the black box: low-dimensional dynamics in high-dimensional recurrent neural networks. *Neural Comput.* **25**, 626–649 (2013).
44. Kambara, H., Shin, D. & Koike, Y. A computational model for optimal muscle activity considering muscle viscoelasticity in wrist movements. *J. Neurophysiol.* **109**, 2145–2160 (2013).
45. Martins, A. R. O. & Froemke, R. C. Coordinated forms of noradrenergic plasticity in the locus coeruleus and primary auditory cortex. *Nat. Neurosci.* **18**, 1483–1492 (2015).
46. Swinehart, C. D. & Abbott, L. F. Supervised learning through neuronal response modulation. *Neural Comput.* **17**, 609–631 (2005).
47. Breakspear, M. Dynamic models of large-scale brain activity. *Nat. Neurosci.* **20**, 340–352 (2017).
48. Mante, V., Sussillo, D., Shenoy, K. V. & Newsome, W. T. Context-dependent computation by recurrent dynamics in prefrontal cortex. *Nature* **503**, 78–84 (2013).
49. Bargmann, C. I. Beyond the connectome: how neuromodulators shape neural circuits. *BioEssays* **34**, 458–465 (2012).
50. Bassett, D. S. & Sporns, O. Network neuroscience. *Nat. Neurosci.* **20**, 353–364 (2017).

Acknowledgements

We thank the members of the Vogels lab (particularly E. J. Agnes, R. P. Costa, W. F. Podlaski, and F. Zenke) for their insightful comments and Y. T. Kimura for creating the monkey illustration. We also thank O. Barak, T. E. J. Behrens, R. Bogacz, M. Jazayeri, and L. Susman for their helpful comments. Our work was supported by grants from the Wellcome Trust (T.P.V. and J.P.S. through WT100000, and G.H. through 202111/Z/16/Z) and the Engineering and Physical Sciences Research Council through the Life Sciences Interface Doctoral Training Centre at the University of Oxford (EP/F500394/1 to J.P.S.).

Author contributions

J.P.S., G.H., and T.P.V. conceived the study and developed the model. J.P.S. performed simulations for Figs. 1–5 and Supplementary Figs. 1–4, and J.P.S. and G.H. performed simulations for Figs. 6–8 and Supplementary Figs. 5–8. J.P.S. analyzed the results, produced the figures, and wrote the first draft of the manuscript. J.P.S., M.A.P., G.H., and T.P.V. discussed and iterated on the analysis and its results, and all authors also revised the final manuscript.

Competing interests

The authors declare no competing interests.

Additional information

Supplementary information is available for this paper at https://doi.org/10.1038/s41593-018-0276-0.

Reprints and permissions information is available at www.nature.com/reprints.

Correspondence and requests for materials should be addressed to J.P.S.

Methods

Model. Our model is specified by a differential equation governing the neuronal activity (equation (1)), the gain function (equation (2)), a set of readout weights, and each neuron's gain. In the following discussions, we describe our model precisely.

Neuronal dynamics. We model neuronal activity according to equation (1), which we integrate using the ODE45 function (using default parameters) in Matlab. We do not explicitly model dynamics before movement execution; all of our simulations begin at the time of movement onset[4,11] (except when we use a ramping input in Fig. 2). We choose the initial condition $\boldsymbol{x}_0$ among the 'most observable' modes of the system (i.e., those that elicit the strongest transient dynamics[11]). Specifically, we first linearize equation (1) around its unique equilibrium point $\boldsymbol{x}=\boldsymbol{0}$ using unit gains (i.e., $g_i=1$ for all i), and we compute the observability Gramian (a symmetric positive-definite matrix $\boldsymbol{Q}$) of the linearized system. The most observable modes are the top eigenvectors of $\boldsymbol{Q}$[11]. Unless we state otherwise, we choose the eigenvector associated with the largest eigenvalue of $\boldsymbol{Q}$ (note that all of its eigenvalues are real and positive) as the initial condition $\boldsymbol{x}_0$ for the neuronal activity. Following ref. [11], we also scale $\boldsymbol{x}_0$ so that $||\boldsymbol{x}_0||_2=1.5\sqrt{N}$.

Biophysical interpretation of equation (1). Equation (1), together with equation (2), describes how we model neuronal firing rates relative to a baseline rate r_0. In this section, we clarify that one can obtain identical neuronal activity by using a strictly positive gain function f and including a constant input $\boldsymbol{h}$ in equation (1). Specifically, given a desired baseline firing rate r_0, one can model the neuronal activity as

$$\tau\frac{d\boldsymbol{x}(t)}{dt}=-\boldsymbol{x}(t)+\boldsymbol{W}f(\boldsymbol{x}(t);\boldsymbol{g})+\boldsymbol{h}\,, \tag{3}$$

for the same initial condition $\boldsymbol{x}_0$ that we described above, where $h_i=-r_0\sum_j W_{ij}$ and

$$f(x_i;g_i)=\begin{cases} r_0\tanh(g_i x_i/r_0)+r_0, & \text{if } x_i<0\,,\\ (r_{\max}-r_0)\tanh(g_i x_i/(r_{\max}-r_0))+r_0, & \text{if } x_i\geq 0\,,\end{cases} \tag{4}$$

where $r_{\max}$ is the maximum firing rate. Note that the constant term $\boldsymbol{h}$ in equation (3) is necessary to balance the additional r_0 term in equation (4).

Construction of the network architecture. Prior to stability optimization (see below), we generate synaptic weight matrices $\boldsymbol{W}$ as detailed in ref. [11]. In keeping with Dale's law, these matrices consist of M positive (excitatory) columns and M negative (inhibitory) columns. We begin with a set of sparse (such that the connection probability between any two neurons is small) and strong weights with nonzero elements set to $w_0/\sqrt{N}$ (excitatory) and $-\gamma w_0/\sqrt{N}$ (inhibitory), where $w_0^2=2\rho^2/(p(1-p)(1+\gamma^2))$ and the connection probability between each two neurons is homogeneous and is given by $p=0.1$. This construction results in $\boldsymbol{W}$ having an approximately circular spectrum (i.e., set of eigenvalues) of radius ρ (which we set to $\rho=10$), leading to linear instability before stability optimization. As in ref. [11], we set the inhibition/excitation ratio γ to be $\gamma=3$.

After constructing the initial $\boldsymbol{W}$, we never change any of the excitatory connections. Following ref. [11], we refine the inhibitory connections to minimize an upper bound of $\boldsymbol{W}$'s 'spectral abscissa' (SA; i.e., the largest real part among the eigenvalues of $\boldsymbol{W}$)[11]. Briefly, we iteratively update inhibitory weights to follow the negative gradient of this upper bound to the SA. First, the inhibitory weights remain inhibitory (i.e., negative). Second, we maintain a constant ratio (of $\gamma=3$) of mean inhibitory weights to mean excitatory weights. Third, we restrict the density of inhibitory connections to be at most 0.4 to maintain sufficiently sparse connectivity. We observed that this constrained gradient descent usually converges within a few hundred iterations. As noted in ref. [11], the SA typically decreases during optimization from 10 to about 0.15. For additional details, see the Supplementary Information of ref. [11].

As a proof of principle, we also construct a chaotic variant of our recurrent neuronal-network model (Fig. 2). These networks are chaotic in the sense that the neuronal dynamics in equation (1) have a positive maximum Lyapunov exponent[51]. We use a synaptic weight matrix $\boldsymbol{W}$ (as described above) before stability optimization, but we now use parameter values of $\gamma=1$ and $\rho=1.5$. We also set $\tau=20$ ms, and we choose the initial condition $\boldsymbol{x}_0$ for the neuronal activity from a uniform distribution on the interval $[-10, 10]$. We use only the first 0.5 s of neuronal activity for our simulations of the chaotic network model.

Creating target muscle activity. We generate target muscle activities of duration $t_{\text{tot}}=500$ ms (Figs. 1–5) and $t_{\text{tot}}=2{,}500$ ms (Figs. 6–8). In each case, we draw muscle activity from a Gaussian process with a covariance function $K\in[0, t_{\text{tot}}]\times[0, t_{\text{tot}}]\rightarrow \mathrm{R}_{\geq 0}$ that consists of a product of a squared-exponential kernel (to enforce temporal smoothness) and a nonstationary kernel that produces a temporal envelope similar to that of real electromyogram (EMG) data during reaching[4]. Specifically,

$$K(t,t')=e^{-\frac{(t-t')^2}{2\ell^2}}\times E(t/\sigma)\times E(t'/\sigma)\,, \tag{5}$$

where $E(t)=te^{(-t^2/4)}$. We set $\sigma=110$ ms and $\ell=50$ ms for movements that last 500 ms, and $\sigma=550$ ms and $\ell=250$ ms for movements that last 2,500 ms. We also multiply the resulting muscle activity by a scalar to ensure that it has the same order of magnitude as the neuronal activity. We use a sampling rate of 400 Hz for movements that last 500 ms and 200 Hz for movements that last 2,500 ms.

We are modeling network output as a proxy for muscle-force activity. When we study whether we can generate the same movement that lasts five times longer (Figs. 6–8), we scale the duration of the muscle activity without changing its amplitude. To actually generate the same movement so that it lasts five times longer, we also need to scale the amplitude of the muscle activity by the factor $1/5^2=1/25$. To demonstrate the effectiveness of learning through gain modulation, we omit this scaling, so the tasks on which we train are more difficult ones, as the target activity without the scaling has a substantially larger amplitude throughout the movement. However, we find that learning through gain modulation can also account for this scaling of muscle activity when performing movements at different speeds (Supplementary Fig. 8). Alternatively, it may be possible for gain modulation of downstream motor neurons in the spinal cord to account for scaling of the amplitude of muscle activity when performing movements at different speeds (for example, see ref. [21]).

Network output. We compute the network output $z(t)$ as a weighted linear combination of excitatory neuronal firing rates:

$$z(t)=\boldsymbol{m}^{\mathrm{T}}f(\boldsymbol{x}^E(t);\boldsymbol{g}^E)+b\,, \tag{6}$$

where $\boldsymbol{m}, \boldsymbol{x}^E(t), \boldsymbol{g}^E\in\mathrm{R}^M$, the quantity $\boldsymbol{x}^E(t)$ is the excitatory neuronal activity, and M is the number of excitatory neurons. To ensure that the network output corresponds to realistic muscle activity (see "Creating target muscle activity") before any training of the neuronal gains, we fit the readout weights $\boldsymbol{m}$ and the offset b to an initial output activity using least-squares regression. To ameliorate any issues of overfitting, we use 100 noisy trials, in which we add white Gaussian noise to the initial condition $\boldsymbol{x}_0$ for each trial with a signal-to-noise ratio of 30 dB[11]. Subsequently, the readout weights remain fixed throughout training of the neuronal gains. See our simulation details for each figure for additional details.

Measuring error in network output. We compute the error ε between the network output $\boldsymbol{z}\in\mathbb{R}^{t_{\text{tot}}}$ and a target $\boldsymbol{y}\in\mathbb{R}^{t_{\text{tot}}}$ by discretizing time and calculating

$$\varepsilon=1-R^2=\frac{\sum_{t=1}^{t_{\text{tot}}}(z(t)-y(t))^2}{\sum_{t=1}^{t_{\text{tot}}}(y(t)-\bar{y})^2}\,, \tag{7}$$

where $\bar{y}=\frac{1}{t_{\text{tot}}}\sum_{t=1}^{t_{\text{tot}}}y(t)$ and R^2 is the coefficient of determination (which is often called simply 'R-squared'). Therefore, an error of $\varepsilon=1$ implies that the performance is as bad as if the output $\boldsymbol{z}$ were equal to the mean of the target $\boldsymbol{y}$ and thus does not capture any variations in output. When we use multiple readout units, we take the mean error ε across all outputs. We use this definition of error throughout the entire paper.

A learning rule for neuronal input–output gains. We devise a reward-based node-perturbation learning rule that is biologically plausible, in the sense that it includes only local information and a single scalar reward signal that reflects a system's recent performance[29,30]. Our learning rule progressively reduces the error (on average) between the network output and a target output over training iterations. We update the gain g_i for neuron i after each training iteration t_n (with $n=1, 2, 3, \ldots$) according to the following learning rule:

$$g_i(t_n)=g_i(t_{n-1})+R(t_{n-1})(g_i(t_{n-1})-\bar{g}_i(t_{n-1}))+\xi_i(t_n)\,, \tag{8}$$

where

$$\begin{aligned} R(t_n)&=sgn(\bar{\varepsilon}(t_{n-1})-\varepsilon(t_n))\,,\\ \bar{\varepsilon}(t_n)&=\alpha\bar{\varepsilon}(t_{n-1})+(1-\alpha)\varepsilon(t_n)\,,\\ \bar{g}_i(t_n)&=\alpha\bar{g}_i(t_{n-1})+(1-\alpha)g_i(t_n)\,,\end{aligned} \tag{9}$$

where $\varepsilon(t_n)$ represents the output error at iteration t_n (see "Measuring error in network output"), sgn is the sign function, $\xi_i(t_n)\sim\mathcal{N}(0, 0.001^2)$ is a Gaussian random variable with mean 0 and s.d. 0.001, and $\alpha=0.3$. The initial modulatory signal is $R(t_0)=0$, and the other initial conditions are $\bar{\varepsilon}(t_0)=\varepsilon(t_0)$ (where $\varepsilon(t_0)$ is the initial error before training) and $\bar{g}_i(t_0)=g_i(t_0)=1$. One can interpret the terms $\bar{g}_i$ and $\bar{\varepsilon}$ as lowpass-filtered gains and errors, respectively, over recent iterations, with a history controlled by the decay rate α[32]. We use these parameter values in all of our simulations in this paper. We find that varying the standard deviation of the noise term ξ or the factor α has little effect on the learning dynamics (not shown), in line with ref. [31].

Although our learning rule in equation (8) is similar to reward-modulated 'exploratory Hebbian' (EH) synaptic plasticity rules[30–32], we investigate changes in

neuronal gains (i.e., the responsiveness of neurons) inside a recurrent neuronal network, rather than synaptic weight changes. The above notwithstanding, we expect our learning rule to perform well for a variety of learning problems. For example, it can solve credit-assignment problems, because one can formulate such a node-perturbation learning rule as reinforcement learning with a scalar reward[52].

The modulatory signal R does not provide information about the sign and magnitude of the error, and it also does not indicate the amount that each readout (if using multiple readouts) contributes to a recent change in performance. The modulatory signal R indicates only whether performance is better or worse, on average, compared with previous trials. One can view the modulatory signal as an abstract model for phasic output of dopaminergic systems in the brain[19,23,24,53].

We use the following procedure for updating neuronal gains. We update the gains for iteration t_1 according to equation (8), and we obtain the network output from the gain pattern $\boldsymbol{g}(t_1)$. We then calculate the error $\varepsilon(t_1)$ from the output, and we subsequently calculate the modulatory signal $R(t_1)$ and the quantities $\bar{\varepsilon}(t_1)$ and $\bar{\boldsymbol{g}}(t_1)$ using equation (9). We then repeat this process for all subsequent iterations. If any gain values become negative, we set these to 0. However, this happened very rarely in our computations, and we observed it only when we used 60,000 training iterations (i.e., in Figs. 3e and 6b).

Alternative learning rule. One can also adapt our learning rule so that learning ceases when the modulatory signal $R(t_n)$ saturates at a sufficiently small value. One can achieve this by instead placing the noise term ξ_i inside the brackets in equation (8), so that ξ_i is multiplied by the modulatory signal R, together with changing the *sgn* function in equation (9) to the tanh function. This yields the following learning rule:

$$g_i(t_n) = g_i(t_{n-1}) + R(t_{n-1})\left(g_i(t_{n-1}) - \bar{g}_i(t_{n-1}) + \xi_i(t_n)\right), \tag{10}$$

where

$$\begin{aligned} R(t_n) &= \tanh\left(\eta\left(\bar{\varepsilon}(t_{n-1}) - \varepsilon(t_n)\right)\right), \\ \bar{\varepsilon}(t_n) &= \alpha\bar{\varepsilon}(t_{n-1}) + (1-\alpha)\varepsilon(t_n), \\ \bar{g}_i(t_n) &= \alpha\bar{g}_i(t_{n-1}) + (1-\alpha)g_i(t_n), \end{aligned} \tag{11}$$

and $\eta = 50{,}000$ controls the slope of the tanh function at 0 (i.e., when the lowpass-filtered error $\bar{\varepsilon}(t_n)$ matches the current error $\varepsilon(t_n)$). Learning now stops when $\bar{\varepsilon}(t_{n-1}) = \varepsilon(t_n)$; see Fig. 2a. We achieve a qualitatively similar learning performance by using equations (10) and (11) instead of equations (8) and (9), respectively (Fig. 2a).

Generating groups for group-based gain modulation. For coarse-grained (i.e., grouped) gain modulation, we generate n (modulatory) groups, and we independently modulate each group using one external 'modulatory unit'. Our generation mechanism for random groups is as follows. For each of the n groups, we choose N/n neurons (where N is the total number of neurons in the network) uniformly at random without replacement. If n does not divide N, we assign the remaining neurons to groups uniformly at random.

When using specialized groupings (Fig. 3b,c and Supplementary Fig. 2a–d) for a particular target movement, we obtain groups by applying k-means clustering (where k is the desired number of groups) to 10 gain patterns that we obtain from 10 prior independent training sessions (using neuron-specific control) on the same target and which correspond to the minimum error for each training session. We thus apply k-means clustering to a matrix of size $N \times 10$, where row i has the gain values for neuron i from the 10 independent training sessions to the same target. Applying k-means clustering then generates groupings in which neurons in the same group tend to have similar gain values following training using neuron-specific modulation.

Simulation details. We now give a brief summary of our simulations for Figs. 1–8. See the Supplementary Math Note for our mathematical derivations. A 'readme' file is also available with full details of our simulations, along with sample Matlab code in the supplementary material. (We have also posted this information at http://modeldb.yale.edu/246004.) Additionally, see the Nature Research Reporting Summary for additional information.

Figure 1. We simulate two different electromyograms (EMGs; see "Creating target muscle activity") of muscle activities (initial reach and target reach) that each last 0.5 s (Fig. 1a,f). We use a network of $N = 200$ neurons and sample transient neuronal firing rates that last 0.5 s following the initial condition $\boldsymbol{x}_0$ of the neuronal activity (see "Neuronal dynamics"). We fit the readout weights over 100 trials, in which we add white Gaussian noise to the initial condition $\boldsymbol{x}_0$ (with a signal-to-noise ratio of 30 dB) using least-squares regression so that the network output, with all gains set to 1, generates the initial reach (see "Network output"). We use the same readout weights throughout all training, and we use only one readout unit for each simulation.

For each training iteration of the neuronal gains (to generate a target movement), we use the initial condition $\boldsymbol{x}_0$ at time $t = 0$. We calculate the subsequent network output as described in the "Network output" section, and we update the neuronal gains according to equation (8). We repeat this process for 18,000 training iterations (which corresponds to 2.5 h of training time), which is enough training time for the error to saturate (Fig. 1d). We run 10 independent training sessions on the same target, and we plot these results in Fig. 1d,e.

Figure 2. We train neuronal gains on the same task as the one that we showed in Fig. 1d using three alternative models. For one model, we use a ramping input to the neuronal activity in equation (1) as a model of preparatory activity before movement onset[4,11]. We use the same ramping input function that was used in ref. [11]. It is $\exp(t/\tau_{on})$ for $t < 0$ s and $\exp(t/\tau_{off})$ after movement onset ($t \geq 0$), with an onset time of $\tau_{on} = 400$ ms and an offset time of $\tau_{off} = 2$ ms. Gain changes that result from learning now also affect the neuronal activity at $t = 0$ (i.e., at movement onset).

We also train a chaotic[34] variant of our model (see "Construction of the network architecture" for a description of how we construct such a model), and we use the first 0.5 s of neuronal activity.

Finally, we use an alternative learning rule (see equations (10) and (11)) in which learning stops automatically when the difference between network output errors in successive training iterations becomes sufficiently small (see "Alternative learning rule").

Figure 3. For Fig. 3b,c, we generate five different target outputs and run 10 independent training sessions for each target. For the random groupings (see "Generating groups for group-based gain modulation"), we use different independently generated random groups for each simulation. For the specialized groups (see "Generating groups for group-based gain modulation"), for a given number of groups, we use the same grouping in all simulations.

We now explain how we determine specialized groups that are shared by multiple movements (i.e., we use the same grouping for learning multiple movements); see Fig. 3c and Supplementary Fig. 2b–d. We apply k-means clustering (where k is the desired number of groups) across all of the gain patterns that we obtain using neuron-specific modulation for each of the movements. That is, we apply k-means clustering to a matrix of size $N \times (10 \times q)$, where N is the number of neurons and q is the number of movements (and, equivalently, the number of gain patterns).

For the task that we just described above, we consider various different numbers of groups (using random groupings) for networks with $N = 100$, $N = 200$, and $N = 400$ neurons. We again perform 10 independent training sessions for each network, target, and number of groups. We fit the readout weights so that each scenario generates the same network output when all gains are set to 1. The readout weights remain fixed throughout training. We plot these results in Fig. 3d and Supplementary Fig. 2e–h.

When we use multiple readout units (Fig. 3e,f), we generate 10 different initial and target outputs for each readout unit. We run independent training sessions for these 10 sets of target outputs and calculate mean errors across the 10 training sessions. For a given number of readout units, we use the same sets of initial and target outputs for all three network sizes and each number of random modulatory groups. We thus fit readout weights so that each scenario generates the same output with all gains set to 1. The readout weights remain fixed throughout training. We use 60,000 (instead of 18,000) training iterations to ensure error saturation.

Figure 4. To create libraries of learned movements, we train a network of 400 neurons and 40 random groups (see "Generating groups for group-based gain modulation") on each of 100 different target movements independently. (In other words, this generates 100 different gain patterns, with one for each movement.) For library sizes of $l \in \{1, 2, \ldots, 50\}$, we choose 100 samples of l movements (from the learned gain patterns and their outputs) uniformly at random without replacement for each l. We then fit the set of l movements in each of the 100 sample libraries using least-squares regression for each of 100 hitherto-untrained novel target movements. We constrain the fitting coefficients c_j from the least-squares regression by requiring that $c_j \geq 0$ for all j and $\sum_{j=1}^{l} c_j = 1$. We calculate the fit error (i.e., the error between the fit and the target), the output error (i.e., the error between the output and the target), and the error between the fit and the output for each of the 100 novel target movements, each of the 100 library samples, and each l. In Fig. 4, we show results for up to $l = 20$ library elements. In Supplementary Fig. 3, we show results for up to $l = 50$ library elements.

Figure 5. We train the same 200-neuron weight matrix that we used in Fig. 1 on the same task as in Fig. 1d–f, except with a baseline rate of $r_0 = 5$ Hz in equation (2). We also repeat the simulations in Fig. 4 for the baseline rate $r_0 = 5$ Hz.

Figure 6. In each of these simulations, we use a network of 400 neurons and 40 random modulatory groups (see "Generating groups for group-based gain modulation"). We construct slow (2.5 s) target movements with $\sigma = 550$ ms and $\ell = 250$ ms in equation (5). We then construct a fast (0.5 s) variant of each movement. Each movement variant has 500 evenly spaced points (see "Creating target muscle activity"). We sample the fast variant using 100 evenly spaced points, and we then augment 400 instances of 0 values to the final 2 s of the movement to ensure that both movement variants have the same length.

For Fig. 6b, we fit readout weights using least-squares regression, such that with all gains set to 1, the network output generates the fast variant. We then train gain patterns using our learning rule in equations (8) and (9) so that the network output generates the slow-movement variant. (The initial condition $\boldsymbol{x}_0$ and readout weights remain fixed.) We use 60,000 training iterations, and we run 10 independent training sessions for each of 10 different target movements.

For Fig. 6c, we perform the task that we described in the paragraph above using a gradient-descent training procedure with gradients that we obtain from back-propagation[54]. Together with learning the gain pattern for the slow variant, we jointly optimize a single set of readout weights (shared by both the fast-movement and slow-movement variants; see "Network output") as part of the same training procedure. The gains are still fixed at 1 for the fast variant. The cost function for the training procedure is equal to the squared Euclidean 2-norm between actual network outputs and the corresponding target outputs (summing the contributions from fast and slow speeds) plus the Euclidean 2-norm of the readout weights, where the latter acts as a regularizer. We run gradient descent for 500 iterations, which is well after the cost has stopped decreasing.

For each of the 10 trained movements that we described earlier in this section, we extract the mean minimum error across all simulations for both the outputs obtained via our learning rule (Supplementary Fig. 5a) and the outputs obtained via back-propagation (Supplementary Fig. 5b). We then linearly interpolate between the learned gain patterns for the fast and slow outputs, and we calculate the error between the output and the target movement at the interpolated speed (Fig. 6d.)

For Fig. 6d–f, we train networks to generate a pair of target movements in response to a corresponding pair of orthogonal initial conditions at fast and slow speeds and also at each of five intermediate, evenly spaced speeds in between these extremes. To do this, we parameterize the gain pattern of speed index s (with $s \in \{1, \ldots, 7\}$) as a convex combination of a gain pattern $\boldsymbol{g}_{s=1}$ for fast movements and a gain pattern $\boldsymbol{g}_{s=7}$ for slow movements, with interpolation coefficients of λ_s (with $\boldsymbol{g}_s = \lambda_s \boldsymbol{g}_{s=1} + (1-\lambda_s)\boldsymbol{g}_{s=7}$, $\lambda_1 = 1$, and $\lambda_7 = 0$). We optimize (using back-propagation, as discussed above) over $\boldsymbol{g}_{s=1}$, $\boldsymbol{g}_{s=7}$, the five interpolation coefficients λ_s (with $s \in \{2, \ldots, 6\}$), and a single set of readout weights. For a given speed s, we use the gain pattern $\boldsymbol{g}_s$ for both movements. We call the collection of gain patterns $\boldsymbol{g}_s$ for $s \in \{1, \ldots, 7\}$ the gain manifold for speed control (i.e., the 'speed manifold').

Figure 7. We train (using back-propagation) a 400-neuron network with 40 random modulatory groups (see "Generating groups for group-based gain modulation") to generate each of 10 different movement shapes at seven different, evenly spaced speeds (ranging from the fast variant to the slow variant) using a fixed initial condition $\boldsymbol{x}_0$. To jointly learn gain patterns that control movement shape and speed, we parameterize each gain pattern as the element-wise product of a gain pattern that encodes shape (which we use at each speed for a given shape) and a gain pattern that encodes speed (which we use at each shape for a given speed). We again parameterize (see our simulation details for Fig. 6) the gain pattern that encodes speed index s (with $s \in \{1, \ldots, 7\}$) as a convex combination of two common endpoints, $\boldsymbol{g}_{s=1}$ (which we use for the fast-movement variants) and $\boldsymbol{g}_{s=7}$ (which we use for the slow-movement variants). We thus optimize over 10 gain patterns for movement shape, two gain patterns each for fast and slow movement speeds, five speed-interpolation coefficients, and a single set of readout weights.

In Fig. 7c, we calculate the mean error between the network output and the target over the 10 target movements when generating gain patterns for movement speed by linearly interpolating between the trained fast ($\boldsymbol{g}_{s=1}$) and slow ($\boldsymbol{g}_{s=7}$) gain patterns.

Figure 8. We use the 10 trained gain patterns for movement shapes, as well as the speed manifold from Fig. 7. (See our simulation details for Fig. 7.) Using our learning rule from equations (8) and (9), we train the 10 coefficients $c_1, \ldots, c_{10}$ (Fig. 8a) to construct a new gain pattern from the 10 existing shape-specific gain patterns that, together with the speed manifold, generates a new target movement at the fast and slow speeds. Specifically, we replace the gains g_i (for $i \in \{1, \ldots, N\}$) with the coefficients c_i (for $i \in \{1, \ldots, 10\}$) in equations (8) and (9). We use the mean of the errors at the fast and slow speeds in the learning rule. To generate the network output at the fast and slow speeds, we calculate the element-wise product between the newly constructed gain pattern and the fast and slow gain patterns, respectively, on the speed manifold. We independently train, using 10,000 training iterations, the coefficients $c_1, \ldots, c_{10}$ on each of the 100 target movements that we used for Fig. 4. As a control, we calculate the mean error between the network output and the target over the 100 target movements when choosing one of the 100 newly learned gain patterns uniformly at random without replacement (Fig. 8c).

Additionally, instead of learning to combine gain patterns using the method that we described in the previous paragraph, we determine coefficients $c_1, \ldots, c_{10}$ using a least-squares regression by fitting the 10 learned movements to each of the 100 target movements at the fast and slow speeds simultaneously and requiring that $c_j \geq 0$ for all j and $\sum_{j=1}^{10} c_j = 1$ (Fig. 8c).

In Fig. 8d, we plot the Pearson correlation coefficient between pairs of target movements versus the Pearson correlation coefficient between corresponding pairs of learned coefficients $c_1, \ldots, c_{10}$. In our visualization, we plot only 1,000 of the 4,950 data points. We choose these points uniformly at random.

Statistics. The only statistical test that we use is a (nonparametric) paired Wilcoxon signed-rank one-sided test in Supplementary Fig. 1e. No statistical methods were used to predetermine sample sizes for our simulations, but our sample sizes are similar to those reported in previous studies[10,11]. There was no experimental randomization in our study because it was a computational study; we had no samples, organisms, or participants.

Reporting Summary. Further information on research design is available in the Nature Research Reporting Summary linked to this article.

Code availability. We include sample Matlab code in the supplementary materials.

References

51. Sompolinsky, H., Crisanti, A. & Sommers, H. J. Chaos in random neural networks. *Phys. Rev. Lett.* **61**, 259–262 (1988).
52. Saito, H., Katahira, K., Okanoya, K. & Okada, M. Statistical mechanics of structural and temporal credit assignment effects on learning in neural networks. *Phys. Rev. E* **83**, 051125 (2011).
53. Frémaux, N. & Gerstner, W. Neuromodulated spike-timing-dependent plasticity, and theory of three-factor learning rules. *Front. Neural Circuits* **9**, 85 (2016).
54. Rumelhart, D. E., Hinton, G. E. & Williams, R. J. Learning representations by back-propagating errors. *Nature* **323**, 533–536 (1986).

nature research

Corresponding author(s): Jake P. Stroud

Reporting Summary

Nature Research wishes to improve the reproducibility of the work that we publish. This form provides structure for consistency and transparency in reporting. For further information on Nature Research policies, see Authors & Referees and the Editorial Policy Checklist.

Statistical parameters

When statistical analyses are reported, confirm that the following items are present in the relevant location (e.g. figure legend, table legend, main text, or Methods section).

n/a	Confirmed	
☐	☒	The exact sample size (*n*) for each experimental group/condition, given as a discrete number and unit of measurement
☒	☐	An indication of whether measurements were taken from distinct samples or whether the same sample was measured repeatedly
☐	☒	The statistical test(s) used AND whether they are one- or two-sided *Only common tests should be described solely by name; describe more complex techniques in the Methods section.*
☒	☐	A description of all covariates tested
☒	☐	A description of any assumptions or corrections, such as tests of normality and adjustment for multiple comparisons
☐	☒	A full description of the statistics including central tendency (e.g. means) or other basic estimates (e.g. regression coefficient) AND variation (e.g. standard deviation) or associated estimates of uncertainty (e.g. confidence intervals)
☒	☐	For null hypothesis testing, the test statistic (e.g. *F*, *t*, *r*) with confidence intervals, effect sizes, degrees of freedom and *P* value noted *Give P values as exact values whenever suitable.*
☒	☐	For Bayesian analysis, information on the choice of priors and Markov chain Monte Carlo settings
☒	☐	For hierarchical and complex designs, identification of the appropriate level for tests and full reporting of outcomes
☒	☐	Estimates of effect sizes (e.g. Cohen's *d*, Pearson's *r*), indicating how they were calculated
☐	☒	Clearly defined error bars *State explicitly what error bars represent (e.g. SD, SE, CI)*

Our web collection on statistics for biologists may be useful.

Software and code

Policy information about availability of computer code

Data collection	We used Matlab 2017a for nearly all simulations. In addition, we used Ocaml programming language when we do gradient-descent through back-propagation that we show in Figures 6 and 7.
Data analysis	We used Matlab 2017a for all analyses.

For manuscripts utilizing custom algorithms or software that are central to the research but not yet described in published literature, software must be made available to editors/reviewers upon request. We strongly encourage code deposition in a community repository (e.g. GitHub). See the Nature Research guidelines for submitting code & software for further information.

Data

Policy information about availability of data

All manuscripts must include a data availability statement. This statement should provide the following information, where applicable:

- Accession codes, unique identifiers, or web links for publicly available datasets
- A list of figures that have associated raw data
- A description of any restrictions on data availability

Data sharing is not applicable to this article as no datasets were generated or analysed for this study.

Field-specific reporting

Please select the best fit for your research. If you are not sure, read the appropriate sections before making your selection.

☒ Life sciences ☐ Behavioural & social sciences ☐ Ecological, evolutionary & environmental sciences

For a reference copy of the document with all sections, see nature.com/authors/policies/ReportingSummary-flat.pdf

Life sciences study design

All studies must disclose on these points even when the disclosure is negative.

Sample size	No statistical methods were used to predetermine sample sizes. Our paper was a computational study and as such, most of the effects we demonstrate produce very small p-values. Therefore, we used sample sizes in our simulations that were sufficient to demonstrate the results but sample sizes were always greater than or equal to 10. We show one p-value in our study which we present in Supplementary Fig. 1e. This p-value is calculated based on 10 training samples (and each sample is composed of the firing rate of 100 neurons). All but 1 of the samples show an increase in mean correlation (generating a p-value of 0.002) where one sample shows a negligible decrease in mean correlation . This was simply used to show an additional result relevant to our study.
Data exclusions	No data were excluded in our study.
Replication	All attempts at replication were successful. Our study was a computational study, and as such, we can re-run simulations by controlling for specific factors. All the results we report were consistently found across many simulations. We also include sample Matlab code in the supplementary material for others to replicate our main results.
Randomization	Randomization is not relevant because our study did not involve group allocation (we had no samples/organisms/participants in our study).
Blinding	Blinding is not relevant because our study did not involve group allocation.

Reporting for specific materials, systems and methods

Materials & experimental systems

n/a	Involved in the study
☒	☐ Unique biological materials
☒	☐ Antibodies
☒	☐ Eukaryotic cell lines
☒	☐ Palaeontology
☒	☐ Animals and other organisms
☒	☐ Human research participants

Methods

n/a	Involved in the study
☒	☐ ChIP-seq
☒	☐ Flow cytometry
☒	☐ MRI-based neuroimaging

SUPPLEMENTARY INFORMATION
https://doi.org/10.1038/s41593-018-0276-0

nature neuroscience

In the format provided by the authors and unedited.

Motor primitives in space and time via targeted gain modulation in cortical networks

Jake P. Stroud[1]*, Mason A. Porter[2,3,4], Guillaume Hennequin[5] and Tim P. Vogels[1]

[1]Centre for Neural Circuits and Behaviour, University of Oxford, Oxford, UK. [2]Department of Mathematics, University of California Los Angeles, Los Angeles, CA, USA. [3]Mathematical Institute, University of Oxford, Oxford, UK. [4]CABDyN Complexity Centre, University of Oxford, Oxford, UK. [5]Computational and Biological Learning Lab, Department of Engineering, University of Cambridge, Cambridge, UK. *e-mail: jake.stroud@cncb.ox.ac.uk

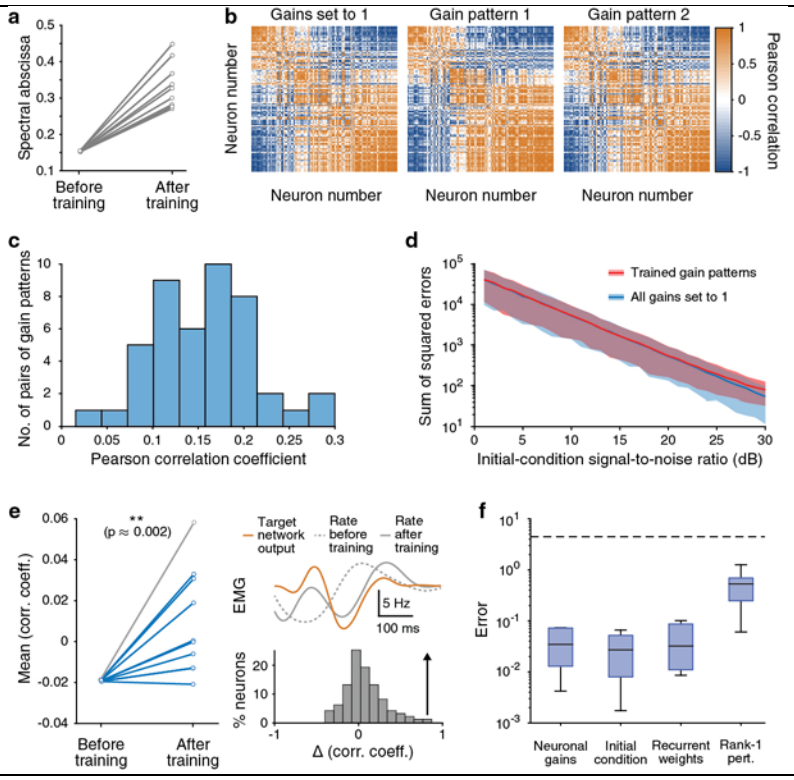

Supplementary Figure 1

Further effects of neuron-specific gain modulation.

a, Changes in the largest real part in the spectrum of $\boldsymbol{W}\times\mathrm{diag}(\boldsymbol{g})$ that result from 10 different training sessions (see our simulation details). Although this change seems substantial, the resulting firing-rate activity does not change dramatically. (For example, see b and the far left panel of Fig. 2b.) **b**, Pearson correlation matrices of the firing rates for all pairs of neurons with (left) all gains set to 1 and (centre and right) two (of the 10) trained gain patterns for the task in Fig. 1d. The order of neurons is the same in all three matrices. Training does not result in a substantial reorganization in Pearson correlations between pairs of neurons. **c**, Histogram of the Pearson correlation coefficients between the 45 pairs of the 10 trained gain patterns for the task in Fig. 1d. **d**, Mean error between the network output with white Gaussian noise added to the initial condition $\boldsymbol{x}_0$ and the network output without noise added to $\boldsymbol{x}_0$ for various signal-to-noise ratios for $1{,}000$ different samples of such noise. We plot results with all gains set to 1 (blue) and the 10 trained gain patterns (red) for the task in Fig. 1d. Shading indicates 1 standard deviation. **e**, Left: The mean Pearson correlation coefficient between the neuronal firing rates and the target increases after training. (We show 10 training sessions, and we use a paired Wilcoxon signed rank one-sided test to generate a p-value of $\mathrm{p} \approx 0.002$.) Bottom right: Example change in Pearson correlation coefficients between the 200 neurons' firing rates and the target after training for the trial in gray in the left panel. Top right: Example of a substantial change in the dynamics of one neuron after training. **f**, Box plots of the errors after training independently on 10 different target movements using back-propagation for four different scenarios. In these examples, we train either the neuronal gains, the initial condition, the recurrent synaptic weight matrix, or a rank-1 perturbation of the synaptic weight matrix. See our full simulation descriptions in the supplementary material). The dashed black line is the mean error over the 10 target movements before training. (Centre lines indicate median errors, boxes indicate 25th to 75th percentiles, whiskers indicate $\pm$ $1.5\times$ the interquartile range, and dots indicate training sessions whose error lies outside the whiskers.

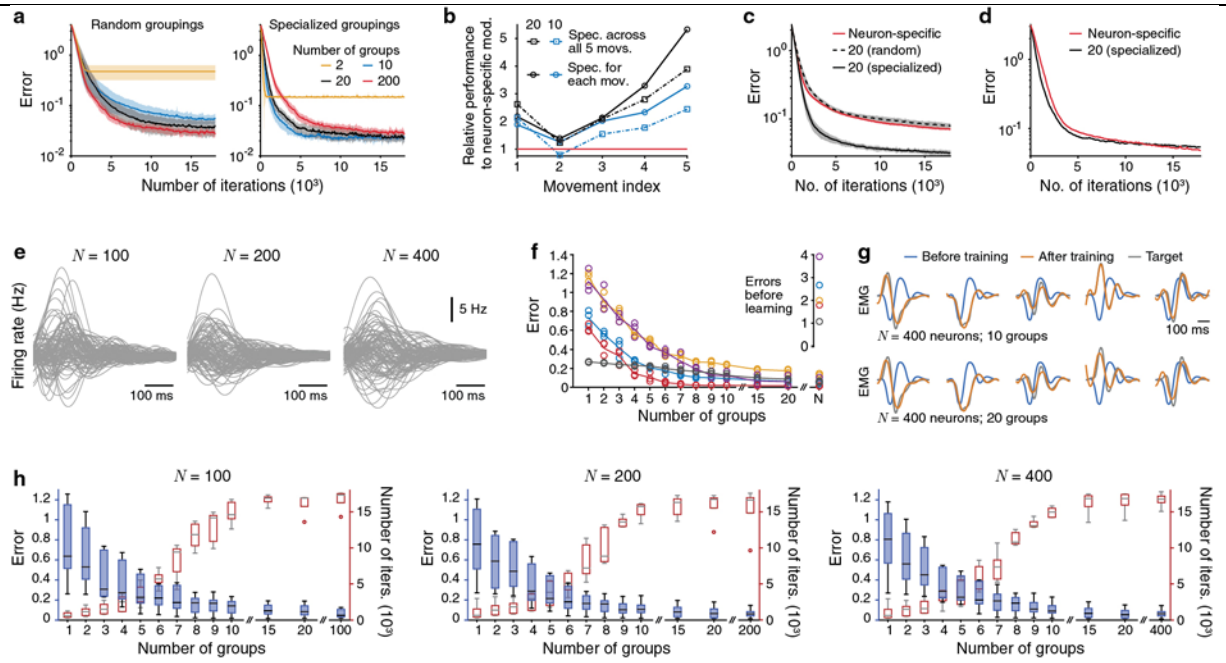

Supplementary Figure 2

Additional results for grouped gain modulation.

a, Mean error over 10 training sessions (where shading indicates one standard deviation) using (left) random and (right) specialized groupings for 2, 10, 20, and 200 (i.e., neuron-specific) groups (see our simulation details). The target output is the same as in Fig. 1. **b**, Relative improvement in performance compared with neuron-specific modulation for each of 5 movements when using specialized groups shared across all (squares) or for each (circles) of the 5 movements using either 10 (blue) or 20 (black) groups. A value of 2 implies that the error is 2 times smaller after training compared to neuron-specific modulation. We indicate the performance of neuron-specific modulation using the red line. **c**, Mean error over 10 training sessions (where shading indicates one standard deviation) when learning 5 movements using either 20 specialized groups (shared across all 5 movements), 20 random groups, or neuron-specific modulation. **d**, Mean error over 10 training sessions when learning 10 novel movements using the specialized grouping (with 20 groups) shared across the 5 previously trained movements from c. **e**, The firing rates of 50 inhibitory and 50 excitatory neurons for each of the three different networks sizes. **f**, The curves give the mean error over 10 training sessions and across the 3 networks for each of 5 targets. The circles represent the mean error for each network, and the different colours indicate each of 5 different target outputs. (See our simulation details and our full simulation descriptions in the supplementary material.) **g**, Outputs for all five targets from the trial that produces the median error for the 400-neuron network for the cases of 10 and 20 groups. **h**, Box plots (in blue) of the minimum error after training for different numbers of groups and the 3 different network sizes. (These are the same data that we plotted in f.) We also include box plots (in red) for the minimum number of iterations required before the error is within 1% of the minimum error. (Center lines indicate median errors, boxes indicate 25th to 75th percentiles, whiskers indicate $\pm$ 1.5$\times$ the interquartile range, and dots indicate training sessions whose error (or number of iterations) lies outside the whiskers.)

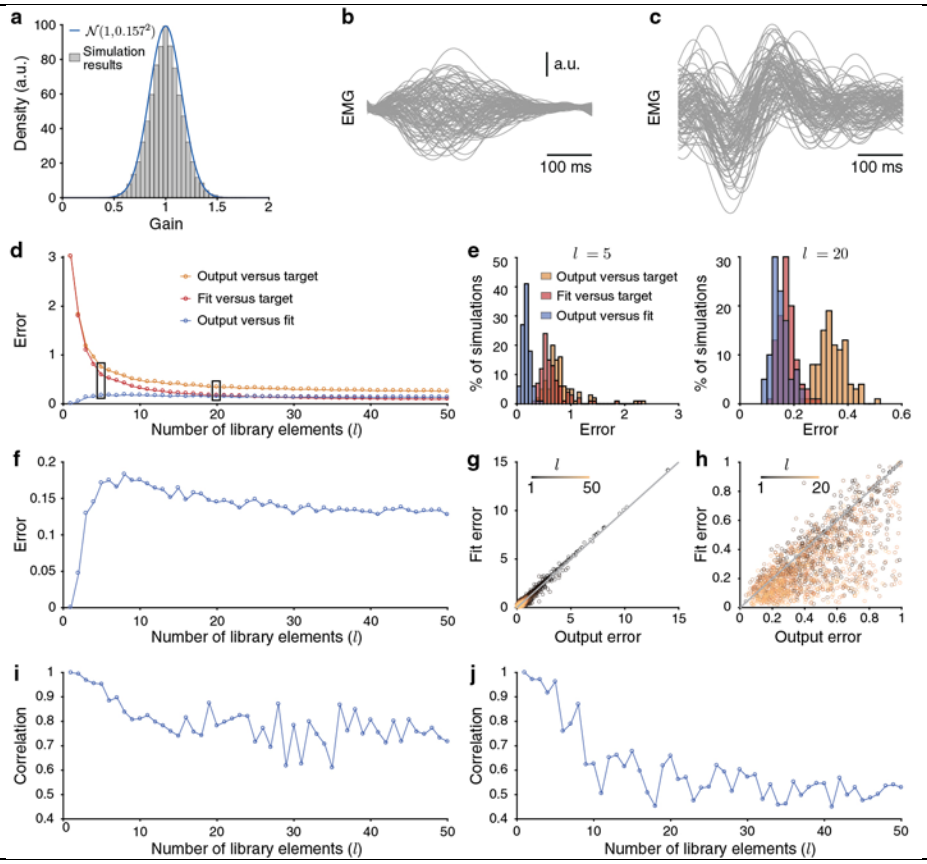

Supplementary Figure 3

Additional results for gain patterns providing motor primitives.

a, The resulting distribution of gains from training independently on each of 100 target outputs (see our simulation details). The distribution of the gain patterns resembles a normal distribution (blue curve) with the same mean and variance as those in Fig. 1e. **b**, Each output from the 100 trained gain patterns. **c**, Outputs of 100 randomly-generated gain patterns from the distribution in a. (See our simulation details and our full simulation descriptions in the supplementary material for further details.) The outputs are substantially more homogeneous than those in b and likely would not constitute a good library for movement generation. **d**, The same plot as in Fig. 4d, but for up to $l = 50$ library elements. **e**, The distributions of errors across 100 different libraries for (left) $l = 5$ and (right) $l = 20$. (Note the difference in horizontal-axis scales in the two plots.) **f**, The error between the output and the fit from d with a different vertical axis scale. **g**, The same plot as in Fig. 4c, but for $l = 1,..., 50$ and with extended axes. Each point represents the 50th-smallest error between the output and the fit across 100 novel target movements for each of 100 randomly-generated combinations of l library elements. We show the identity line in gray. **h**, The same as in g, but each point represents the 50th-smallest error between the output and the fit across the 100 libraries for each of the 100 novel target movements. We plot these data in the square $[0, 1] \times [0, 1]$ and for $l = 1,..., 20$. **i**, For the data in g, we plot the Pearson correlation coefficient between the output and the fit errors over the 100 randomly-generated libraries for each number of library elements (up to $l = 50$). **j**, For the data in h, we plot the Pearson correlation coefficient between the output and the fit errors over the 100 novel target movements for each number of library elements (up to $l = 50$).

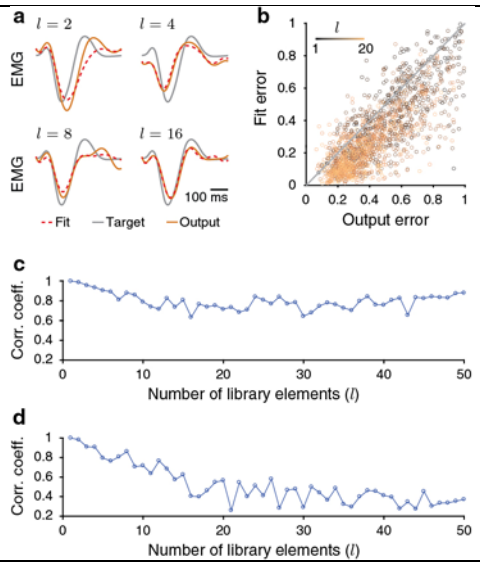

Supplementary Figure 4

Gain patterns as motor primitives with r_0 = 5 Hz.

a, Example target (gray), fit (dashed red), and output (orange) that produces the 50th-smallest output error over 100 randomly-generated combinations (see our simulation details for a description of the generation process) of l library elements using $l = 2$, $l = 4$, $l = 8$, and $l = 16$. **b**, Fit error versus the output error for 100 randomly-generated combinations of l library elements for $l = 1,\ldots, 20$. Each point represents the 50th-smallest error between the output and the fit across 100 novel target movements. We show the identity line in gray. **c**, For the data in b, we plot the Pearson correlation coefficient between the output and the fit errors over the 100 randomly-generated combinations of library elements for each number of library elements (up to $l = 50$). **d**, The same as c, but for data corresponding to the 50th-smallest error for each of the 100 novel target movements, rather than for each randomly-generated combination of library elements (up to $l = 50$) (see our simulation details). Compare c and d of this figure with i and j in Supplementary Fig. 3.

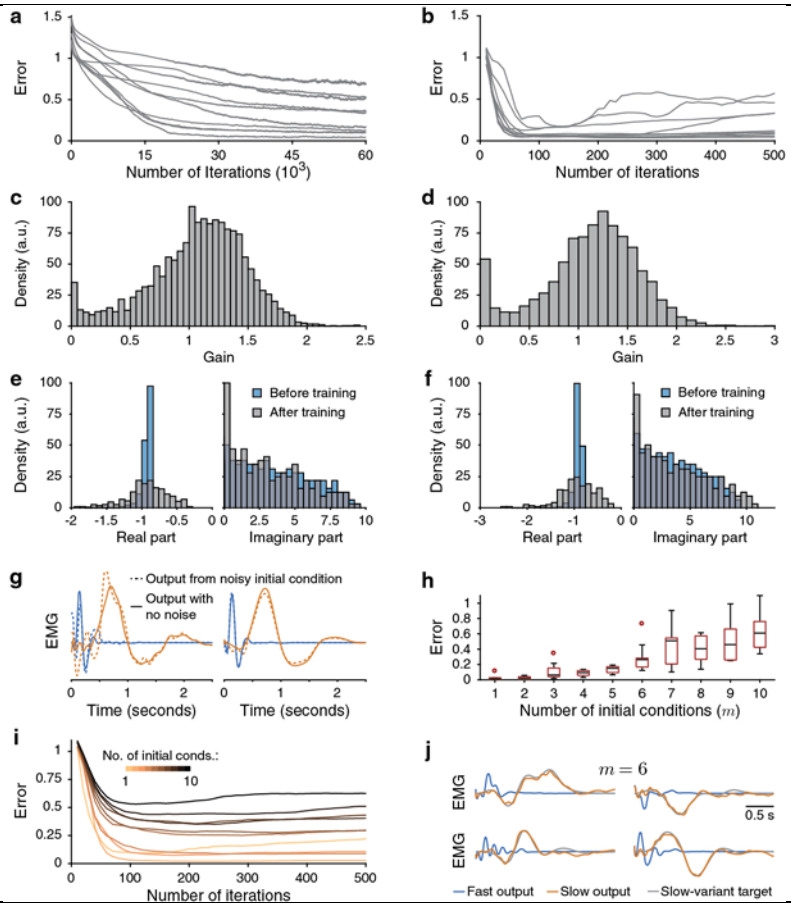

Supplementary Figure 5

Additional results for controlling movement speeds through gain modulation.

a, Mean error over 10 training sessions for each of 10 different movements when learning gain patterns for slow-movement variants using our reward-based learning rule (see our simulation details). **b**, Mean error over 10 training sessions for the same 10 movements when instead learning gain patterns for slow-movement variants using a back-propagation algorithm (see our simulation details). **c**, Distribution of gains for the slow-movement variants across all training sessions using our reward-based learning rule. **d**, Distribution of gains for the slow-movement variants across all training sessions when using back-propagation. **e**, Histograms of the real and imaginary parts of the eigenvalues of the linearization of equation (1) around $\boldsymbol{x} = \mathbf{0}$ before and after training using our reward-based rule for the example in Fig. 6b. **f**, Histograms of the real and imaginary parts of the eigenvalues of the linearization of equation (1) around $\boldsymbol{x} = \mathbf{0}$ before and after training using the back-propagation algorithm for the example in Fig. 6c. **g**, On the left and right, respectively, we show the same outputs that we plotted in Figs. 6b and 6c, but we now add white Gaussian noise (with a signal-to-noise ratio of 4 dB) to the initial condition of the neuronal activity. (See our full simulation descriptions in the supplementary material.) **h**, Box plot of the slow-variant errors across 10 training sessions after training for different numbers of initial conditions. (Center lines indicate median errors, boxes indicate 25th to 75th percentiles, whiskers indicate $\pm$ $1.5\times$ the interquartile range, and dots indicate training sessions whose error lies outside the whiskers.) (See our full simulation descriptions in the supplementary material for further details.) **i**, Mean error during training over 10 training sessions for $m = 1,\ldots, 10$ initial conditions. **j**, For the case of 6 initial conditions in panel (h), we plot 4 example outputs that correspond to the 5th-smallest error for the 10 training sessions. (For each simulation in this figure, we train a 400-neuron network using 40 random modulatory groups; see our simulation details).

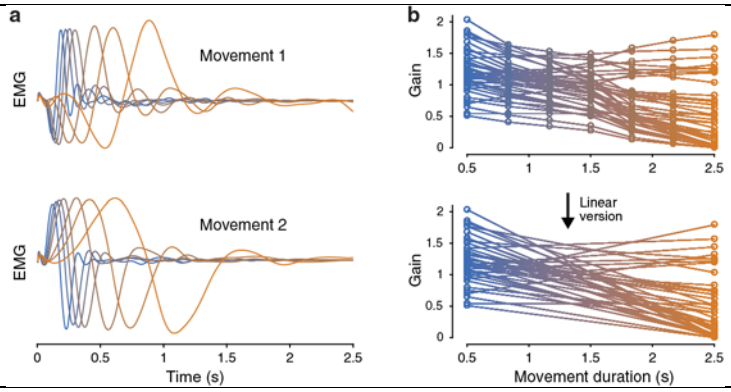

Supplementary Figure 6

Additional results for smooth control of movement speeds through gain modulation.

a, We show outputs that result from the 7 trained gain patterns from Fig. 6e (which we also reproduce here in b) for both initial conditions (see our simulation details). **b**, Top: We reproduce the 7 optimized gain patterns for all 40 modulatory groups when training at 7 evenly spaced speeds from Fig. 6e. We call this the 'speed manifold' in the main text. Bottom: We linearly interpolate between the fast and the slow gain patterns. We use this interpolation for the outputs that we show in Fig. 6f.

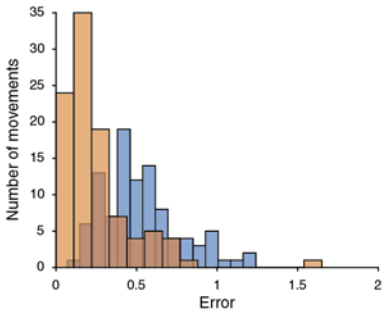

Supplementary Figure 7

Additional results for learning gain-pattern primitives to control movement shape and speed.

We plot histograms of the errors over the 100 target movements from Fig. 8 at both fast (blue) and slow (orange) speeds (see our simulation details).

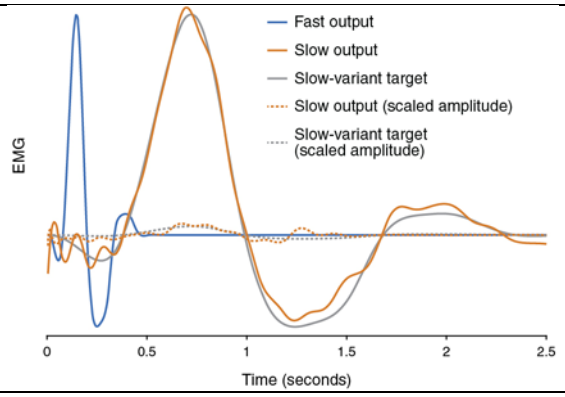

Supplementary Figure 8

Learning slow-movement variants when scaling both the amplitude and duration of target movements.

We can perform the same task as the one that we showed in Fig. 6b when we also scale the amplitude of the slow-variant target movement by the factor $1/25$ (see the dashed curves). Scaling the slow-variant target movement by this factor corresponds to the same movement, but it lasts 5 times longer (see "Creating target muscle activity in Methods). We also reproduce the results from the top panel of Fig. 6b (solid curves) for comparison. During training, we reduce the errors from approximately 128 to 0.9 (i.e., a 99.3% reduction) for the amplitude-scaled task and from approximately 1.22 to 0.02 (i.e., a 98.36% reduction) for the amplitude-fixed task. The error for the amplitude-scaled task is larger than that for the amplitude-fixed task, because we scale the error by the total sum of squared errors of the target. (See equation (7) for the definition of error that we use.)

SUPPLEMENTARY INFORMATION

Supplementary math note

Analysis of the effects of identically changing the gain of all neurons

To examine the effects of gain modulation on neuronal dynamics when identically changing all neuronal gains (i.e., $g_i = g$ for all i), we construct a Taylor expansion of $f(x_i; g_i)$ from Eqn. (2) around $\boldsymbol{x} = \boldsymbol{0}$. By keeping only leading-order terms, we obtain $f(x_i; g) \approx g x_i$, and substituting this expression into Eqn. (1) yields $\tau \dot{\boldsymbol{x}} = (g\boldsymbol{W} - \boldsymbol{I}) \cdot \boldsymbol{x} = \boldsymbol{A} \cdot \boldsymbol{x}$, where $\boldsymbol{I}$ is the identity matrix and $\boldsymbol{A} = g\boldsymbol{W} - \boldsymbol{I}$. Empirically, we find this linear approximation to be valid in a large basin of attraction around the equilibrium point.

Changing the gain from g to g' multiplies the imaginary part of the spectrum of $\boldsymbol{A}$ by the factor g'/g. (Subtracting the identity matrix does not affect the imaginary part of the spectrum of $\boldsymbol{A}$.) This, in turn, multiplies the frequency of the associated solution of the linearized dynamics of $\boldsymbol{x}(t)$ by the factor of g'/g.

A change in gain also causes changes in the real parts of the eigenvalues of $\boldsymbol{A}$. Specifically, increasing the gain causes the real parts of all but one of the eigenvalues of $g\boldsymbol{W}$ to increase (i.e., the eigenvalues of $\boldsymbol{A}$ get closer to the imaginary axis), generally causing a slower decay of activity towards the equilibrium [1]. The real part of the remaining eigenvalue, which is associated with the eigenvector $(1, 1, \ldots, 1)^\top/\sqrt{N}$ (see Ref. [2]), becomes more negative with increasing gain, resulting in faster decay of the neuronal dynamics. However, this effect is small in comparison with the slowing of the decay due to the changes of the real parts of all of the other eigenvalues.

Analysis of linear combinations of gain patterns and their associated neuronal dynamics

In Fig. 4 and Supplementary Figs. 3 and 4, we illustrated that there is a consistent mapping between learned gain patterns and their outputs. Specifically, we illustrated that for a library of l gain patterns $(\boldsymbol{g}_1, \ldots, \boldsymbol{g}_l)$, a convex combination $c_1 F(\boldsymbol{g}_1) + \ldots + c_l F(\boldsymbol{g}_l)$ (so $c_j \geq 0$ for all j and $\sum_{j=1}^{l} c_j = 1$) of their corresponding outputs (which we denote by F) approximates the output $F(c_1\boldsymbol{g}_1 + \ldots + c_l\boldsymbol{g}_l)$ that we obtain by combining the gain patterns with the same coefficients (see Fig. 4). Note that the subscript index j denotes the library element j and is not a neuron index. We now provide some mathematical understanding of this approximation by studying linearized solutions of the neuronal dynamics. Because the network output is a linear combination of the neuronal firing rates, it is sufficient to study convex combinations of internal neuronal activity $\boldsymbol{x}$ directly, rather than convex combinations of network outputs.

For a convex combination (i.e., a weighted mean) of l vectors or matrices $\boldsymbol{\phi}$ with weights c_j, it is

convenient to use the following notation:

$$\mathcal{C}\left[\tilde{\boldsymbol{\phi}}\right] = \sum_{j=1}^{l} c_j \boldsymbol{\phi}_j \,, \tag{12}$$

where the tilde in the square brackets is a reminder that we are summing over the index of the associated library terms. For a given gain pattern $\boldsymbol{G}_j \in \mathbb{R}^{N\times N}$ (where the neuronal gains are elements along the diagonal of $\boldsymbol{G}_j$ (that is, $\boldsymbol{G}_j = \mathrm{diag}(\boldsymbol{g}_j)$), all other elements are 0, and the index j denotes library element j), the solution $\boldsymbol{x}_j(t) \in \mathbb{R}^N$ of the linearized dynamics of Eqn. (1) around $\boldsymbol{x} = \boldsymbol{0}$ is given by

$$\boldsymbol{x}_j(t) = e^{\frac{t}{\tau}(\boldsymbol{W}\boldsymbol{G}_j - \boldsymbol{I})}\boldsymbol{x}_0 \,, \tag{13}$$

under the assumption that there are N distinct eigenvectors for the matrix $\boldsymbol{W}\boldsymbol{G}_j - \boldsymbol{I}$ and that we are away from any bifurcations. Let

$$\boldsymbol{u}(t) = e^{\frac{t}{\tau}(\boldsymbol{W}\mathcal{C}[\tilde{\boldsymbol{G}}] - \boldsymbol{I})}\boldsymbol{x}_0 \tag{14}$$

denote the neuronal activity that results from a convex combination $\mathcal{C}\left[\tilde{\boldsymbol{G}}\right]$ of gain patterns. We need to show that $\boldsymbol{u}(t)$ is approximately the same as the convex combination of the individual neuronal dynamics $\boldsymbol{x}_j(t)$ with the same coefficients c_j. That is, we need to show that the difference

$$\boldsymbol{\Delta}(t) = \boldsymbol{u}(t) - \mathcal{C}\left[\tilde{\boldsymbol{x}}(t)\right] \tag{15}$$

is small with respect to the magnitude of the neuronal activity. We first note that $\frac{d\boldsymbol{\Delta}}{dt}\big|_{t=0} = \boldsymbol{0}$, which we prove as follows:

$$\begin{aligned}
\frac{d}{dt}\boldsymbol{u}(t)\bigg|_{t=0} &= \frac{1}{\tau}\left(\boldsymbol{W}\mathcal{C}\left[\tilde{\boldsymbol{G}}\right] - \boldsymbol{I}\right)\boldsymbol{x}_0 \\
&= \frac{1}{\tau}\mathcal{C}\left[\boldsymbol{W}\tilde{\boldsymbol{G}} - \boldsymbol{I}\right]\boldsymbol{x}_0 \\
&= \frac{d}{dt}\mathcal{C}\left[\tilde{\boldsymbol{x}}(t)\right]\bigg|_{t=0} \,,
\end{aligned} \tag{16}$$

where we used the fact that $\sum_{j=1}^{l} c_j = 1$ to go from the first to the second line, and we note that the matrices $\boldsymbol{W}$ and $\boldsymbol{I}$ do not depend on the gain patterns.

To see whether we can also expect $\boldsymbol{\Delta}(t)$ to be small for $t > 0$, it is useful to consider the power-series expansion of the matrix exponentials on the right-hand side of Eqn. (15):

$$\mathcal{C}\left[\tilde{\boldsymbol{x}}(t)\right] = \mathcal{C}\left[\left(\sum_{m=0}^{\infty}\frac{(\boldsymbol{W}\tilde{\boldsymbol{G}} - \boldsymbol{I})^m}{m!}\right)^{\frac{t}{\tau}}\boldsymbol{x}_0\right] \,, \tag{17}$$

$$\boldsymbol{u}(t) = \left(\sum_{m=0}^{\infty}\frac{\left(\boldsymbol{W}\mathcal{C}\left[\tilde{\boldsymbol{G}}\right] - \boldsymbol{I}\right)^m}{m!}\right)^{\frac{t}{\tau}}\boldsymbol{x}_0 \,. \tag{18}$$

We observe in numerical simulations (not shown) that power-series expansions of this form are accurate descriptions of the associated neuronal dynamics up to second order in m. We therefore truncate to $m = 2$, and we evaluate the difference of Eqns. (17) and (18):

$$\boldsymbol{\Delta}(t) = \left(\frac{1}{2}\right)^{\frac{t}{\tau}} \left(\mathcal{C}\left[\left((\boldsymbol{W}\tilde{\boldsymbol{G}})^2 + \boldsymbol{I} \right)^{\frac{t}{\tau}} \right] - \left(\left(\boldsymbol{W}\mathcal{C}\left[\tilde{\boldsymbol{G}}\right] \right)^2 + \boldsymbol{I} \right)^{\frac{t}{\tau}} \right) \boldsymbol{x}_0 \,. \tag{19}$$

We need to check if the right-hand side of Eqn. (19) is small compared to the neuronal dynamics (i.e., compared to Eqn. (17)). One way to check if this holds at certain times t is to substitute values of t into Eqns. (19) and (17) and calculate the ratio of the norms of these two expressions. Setting $t = \tau$ — at $t = \tau = 200$ ms, the neuronal dynamics are close having reached their maximum amplitude (see Supplementary Fig. 2e) — yields

$$\begin{aligned} \frac{\| \boldsymbol{\Delta}(t)\,|_{t=\tau} \|}{\| \mathcal{C}\left[\tilde{\boldsymbol{x}}(t)\,|_{t=\tau}\right] \|} &\approx \frac{\left\| \left(\mathcal{C}\left[\left(\boldsymbol{W}\tilde{\boldsymbol{G}} \right)^2 + \boldsymbol{I} \right] - \left(\boldsymbol{W}\mathcal{C}\left[\tilde{\boldsymbol{G}}\right] \right)^2 - \boldsymbol{I} \right) \boldsymbol{x}_0 \right\|}{\left\| \left(\mathcal{C}\left[\left(\boldsymbol{W}\tilde{\boldsymbol{G}} \right)^2 + \boldsymbol{I} \right] \right) \boldsymbol{x}_0 \right\|} \\ &= \frac{\left\| \left(\mathcal{C}\left[\left(\boldsymbol{W}\tilde{\boldsymbol{G}} \right)^2 \right] - \left(\mathcal{C}\left[\boldsymbol{W}\tilde{\boldsymbol{G}} \right] \right)^2 \right) \boldsymbol{x}_0 \right\|}{\left\| \left(\mathcal{C}\left[\left(\boldsymbol{W}\tilde{\boldsymbol{G}} \right)^2 \right] + \boldsymbol{I} \right) \boldsymbol{x}_0 \right\|} \,. \end{aligned} \tag{20}$$

We now study the magnitude of the numerator and the denominator of Eqn. (20) and show that the ratio of the former to the latter is small. Both the numerator and the denominator scale approximately in linear proportion to the norm of the product of $\boldsymbol{W}^2$ and $\boldsymbol{x}_0$. (The identity matrix in the denominator is small compared to $\boldsymbol{W}^2$.) The main difference between the numerator and denominator is their dependencies on the gain patterns $\boldsymbol{G}_j$. The numerator scales approximately proportionally to a 'weighted variance' of the gain patterns, whereas the denominator scales approximately proportionally to a weighted mean of the squared gain patterns. Because our learned gain patterns are typically narrowly distributed, with a mean of 1 and approximate standard deviation of 0.15 (see Supplementary Fig. 3a), this ratio is small (on the order of 10^{-2}). Numerically, we confirm that the normalized error in Eqn. (20) is indeed small, which also corroborates the results of Fig. 4 of the main text.

Finally, although we restricted our discussion above to a linear gain function, we note that our numerical simulations suggest that Eqn. (15) is also small for the nonlinear gain function of Eqn. (2) (see Fig. 4 and Fig. 5f) that we used throughout the main text.

REFERENCES

1. G. Teschl, *Ordinary Differential Equations and Dynamical Systems*. American Mathematical Society, 2012.

2. G. Hennequin, T. P. Vogels, and W. Gerstner, "Optimal control of transient dynamics in balanced networks supports generation of complex movements," *Neuron*, vol. 82, no. 6, pp. 1394–1406, 2014.

FULL SIMULATION DETAILS

Simulation details for Fig. 1 and Supplementary Fig. 1

We simulate two different electromyograms (EMGs) (see Methods Section 1.4) of muscle activities (initial reach and target reach) that each last 0.5 s (see Figs. 1a,f). We use a network of $N = 200$ neurons and sample transient neuronal firing rates that last 0.5 s following the initial condition $\boldsymbol{x}_0$ of the neuronal activity (see Methods Section 1.1). We fit the readout weights over 100 trials, in which we add white Gaussian noise to the initial condition $\boldsymbol{x}_0$ (with a signal-to-noise ratio of 30 dB) using least-squares regression so that the network output, with all gains set to 1, generates the initial reach (see Methods Section 1.5). We use the same readout weights throughout all training, and we use only one readout unit for each simulation.

In Fig. 1c, we plot the dynamics of three example neurons with all gains set to 1 (black) and all gains set to 2 (blue).

For each training iteration of the neuronal gains (to generate a target movement), we use the initial condition $\boldsymbol{x}_0$ at time $t = 0$ (see Methods Section 1.1). We calculate the subsequent network output as described in Methods Section 1.5, and we update the neuronal gains according to Eqn. (8). We repeat this process for $18,000$ training iterations (which corresponds to 2.5 hours of training time), which is enough training time for the error to saturate (see Fig. 1d).

We run 10 independent training sessions on the same target, and we plot these results in Figs. 1d,e. For each of the 10 trained gain patterns $\boldsymbol{g}$, we plot the change in the spectral abscissa of $\boldsymbol{W} \times \text{diag}(\boldsymbol{g})$ (i.e., the largest real part in the spectrum of $\boldsymbol{W} \times \text{diag}(\boldsymbol{g})$) in Supplementary Fig. 1a. We observe an increase in the spectral abscissa after training. Although this change seems substantial, the resulting firing-rate activity does not change dramatically (see Supplementary Fig. 1b).

Additionally, we generate 100 network outputs for each of the 10 trained gain patterns using 100 different instances of white Gaussian noise added to the initial condition $\boldsymbol{x}_0$ with a signal-to-noise ratio of s dB (where we consider values of s between 1 and 30 dB in increments of 1). We then calculate the square of the Euclidean 2-norm between each network output and the network output that we obtain when we do not add noise to the initial condition. We call these squared errors $\boldsymbol{e}_1$. (This vector has $1,000$ entries, with one entry for each network output.) We also generate $1,000$ outputs with all gains set to 1 using $1,000$ different instances of white Gaussian noise added to the initial condition $\boldsymbol{x}_0$ with a signal-to-noise ratio of s dB. (We again consider values of s between 1 and 30 dB in increments of 1.) We then calculate the square of the Euclidean 2-norm between each of these network outputs and the network output that we obtain with all gains set to 1 and no noise added to the initial condition. We call these squared errors $\boldsymbol{e}_2$. For each signal-to-noise ratio s, we plot the mean and standard deviation of $\boldsymbol{e}_1$ (i.e., the squared error corresponding to the trained gain patterns) in red and $\boldsymbol{e}_2$ (i.e., the squared error corresponding to all gains set to 1) in blue in Supplementary Fig. 1d. We obtain very similar errors for both the trained and untrained (i.e., all gains set to 1) gain patterns, except for large (i.e., approximately larger than 25 dB) signal-to-noise ratios. For the outputs that we show in Fig. 1f, we add white Gaussian noise to the initial condition

$\boldsymbol{x}_0$ with a signal-to-noise ratio of 30 dB using one of the trained gain patterns and with all gains equal to 1.

To generate the correlation matrices that we show in Supplementary Fig. 1b, we calculate the Pearson correlation coefficient of the neuronal firing rates between all pairs of neurons in the recurrent neuronal network. Therefore, each entry in the matrix indicates the extent to which the neuronal firing rates are similar for a pair of neurons over the duration of the movement (i.e., 0.5 s). In Supplementary Fig. 1b, we show correlation matrices for examples in which all gains are set to 1 and for two example learned gain patterns. We use the same initial condition $\boldsymbol{x}_0$ that we used during training.

We also study whether neuronal firing rates correlate more positively with a target movement after training than before training. To quantify the similarity between the neuronal firing rates and the target output, we calculate — for each of the 10 training sessions that we used in Fig. 1d — the Pearson correlation coefficient of the neuronal firing rates between each neuron and the target output. In Supplementary Fig. 1e, we plot the mean Pearson correlation coefficient across all neurons for the case in which all gains are set to 1 (i.e., before training) and for each of the 10 learned gain patterns (i.e., after training). There is a significant (with a p-value of $p \approx 0.002$) change in the mean Pearson correlation coefficient before training versus after training using a paired Wilcoxon signed rank one-sided test. For the gain pattern that produces the largest change in the mean correlation coefficient (we show this with the grey line in the left panel of Supplementary Fig. 1e), we plot the distribution of changes in the correlation coefficients for all neurons in the bottom right panel of Supplementary Fig. 1e. We see that most values are larger than 0, so the neuronal firing rates become more positively correlated with the target output after learning. We also show an example of a substantial change in the neuronal firing rate of one neuron in the top right panel of Supplementary Fig. 1e.

In another computational experiment, we generate 10 different target muscle activities (see Methods Section 1.4) and, independently for each movement, we train either the neuronal gains, the recurrent synaptic weight matrix $\boldsymbol{W}$, the initial condition $\boldsymbol{x}_0$, or a rank-1 perturbation of the recurrent synaptic weight matrix using a gradient-descent training procedure (with gradients that we obtain from back-propagation [1]). Before training, we use the 200-neuron stability-optimised network, initial condition $\boldsymbol{x}_0$, and readout weights that we used in Fig. 1. Specifically, before any training, the network output is the black curve that we show in Fig. 1f. The cost function for the training procedure is the squared error between the network output and the target movement scaled by the total sum of squares of the target movement (i.e., Eqn. (7)). We run the gradient-descent training procedure until the difference between the cost function at successive training iterations is below 10^{-5} (i.e., until the cost saturates to a small value). When we train the recurrent synaptic weight matrix $\boldsymbol{W}$, after each weight update, we set any positive inhibitory weights to zero and we set any negative excitatory weights to zero. For the rank-1 perturbation, we independently train vectors $\boldsymbol{u}, \boldsymbol{v} \in \mathbb{R}^{200\times 1}$ to reduce the error between the network output, which we obtain from the neuronal firing rates in Eqn. (1) with $\boldsymbol{W}$ replaced by $\boldsymbol{W} + \boldsymbol{u}\boldsymbol{v}^\top$, and the target movement. Before training, the elements of $\boldsymbol{u}$ and $\boldsymbol{v}$ are chosen from a Gaussian distribution with a mean 0 and standard deviation 0.05. In Supplementary Fig. 1f, we plot the errors for 10 different target movements

for each of our 4 different training approaches.

Simulation details for Fig. 2

For this figure, we train neuronal gains on the same task as the one that we showed in Fig. 1d — that is, we independently train 10 gain patterns to generate the target output that we showed in orange in Fig. 1f — using 3 alternative models. We use neuron-specific modulation for these simulations. (This contrasts with our group-based gain modulation.) We fit the readout weights so that, prior to any training (i.e., with all gains set to 1), the network output is the same in each model. (See the black curve in Fig. 1f.) We show the mean error during training in Fig. 2a. The red curve is the same error curve that we plotted in Fig. 1d, but we now use a logarithmic vertical-axis scale.

We also train the neuronal gains on the same task as above, but now using a ramping input to the network (to simulate preparatory activity prior to movement onset [2, 3]). We use the same ramping input function as the one that was used in Ref. [2]. It is $\exp(t/\tau_{\text{on}})$ for $t < 0$ s and $\exp(-t/\tau_{\text{off}})$ after movement onset ($t \geq 0$), with an onset time of $\tau_{\text{on}} = 400$ ms and an offset time of $\tau_{\text{off}} = 2$ ms. Gain changes that result from learning now also affect the neuronal activity at $t = 0$ (i.e., at movement onset). We again run 10 independent training sessions, and we observe results that are qualitatively similar to those we saw in Fig. 1d. (See the blue curve in Fig. 2a.)

We also train a 'chaotic' [4] variant of our model (see Methods Section 1.3, where we describe how we construct such a model), and we train on the same target movement that we mentioned above. We use the first 0.5 s of neuronal activity. We observe a very similar error reduction over training iterations (see the grey curve in Fig. 2a) as we saw in Fig. 1d. (Compare the grey and red curves in Fig. 2a.)

Finally, we use an alternative learning rule (see Eqns. (10) and (11)) in which learning stops automatically when the difference between network outputs over successive training iterations becomes sufficiently small (see Methods Section 1.7). In Fig. 2a, we plot the error reduction using this alternative learning rule in purple. Using this alternative learning rule, we obtain a smaller error for this task (compare the purple and red curves in Fig. 2a), and learning stops after approximately $10,000$ training iterations on average.

In Fig. 2b, we plot the firing rates of 4 example neurons for each of these 4 models both before and after training the neuronal gains.

Simulation details for Fig. 3 and Supplementary Fig. 2

For the same task as in Fig. 1, we plot the results of using random and specialized groupings (see Methods Section 1.9), as well as the neuron-specific result from Fig. 1d, in Supplementary Fig. 2a. We use the same readout weights that we used in Fig. 1.

We now give details for Figs. 3b,c and Supplementary Figs. 2b–d. We generate 5 different target outputs and run 10 independent training sessions for each target. For the random groupings (see Methods Section 1.9), we use different independently-generated random groups for each simulation. For the specialized groups (see Methods Section 1.9), for a given number of groups, we use the same grouping in all simulations. We plot the results of using 10 or 20 groups with either random or specialized groups in Figs. 3b,c and Supplementary Figs. 2b,c.

We now explain how we determine specialized groups that are shared by multiple movements (i.e., we use the same grouping for learning multiple movements); see the plots in Fig. 3c and Supplementary Figs. 2b–d. We apply k-means clustering (where k is the desired number of groups) across all of the gain patterns that we obtain using neuron-specific modulation for each of the movements. That is, we apply k-means clustering to a matrix of size $N \times 10 \cdot q$, where N is the number of neurons and q is the number of movements (and, equivalently, the number of gain patterns). We also use the specialized grouping that we obtain for 20 groups that is shared across 5 movements (see Supplementary Figs. 2b) to learn 10 hitherto-untrained movements. We plot these results in Supplementary Fig. 2d.

For the task that we just described above, we consider various different numbers of groups (using random groupings) for networks with $N = 100$, $N = 200$, and $N = 400$ neurons. We again perform 10 independent training sessions for each network, target, and number of groups. We fit the readout weights so that each scenario generates the same network output when all gains are set to 1. The readout weights remain fixed throughout training. We plot these results in Fig. 3d and Supplementary Figs. 2e–h.

We now give details for Figs. 3e,f. When we use multiple readout units, we generate 10 different initial and target outputs for each readout unit. For example, for 2 readout units, we generate 10 different initial and target outputs for each of units 1 and 2. We run independent training sessions for these 10 sets of target outputs and calculate mean errors across the 10 training sessions. For a given number of readout units, we use the same sets of initial and target outputs for all 3 network sizes and each number of random modulatory groups. We thus fit readout weights so that each scenario generates the same output with all gains set to 1. The readout weights remain fixed throughout training. We use $60,000$ (instead of $18,000$) training iterations to ensure error saturation.

Simulation details for Figs. 4, 5f, and Supplementary Figs. 3,4

To create libraries of learned movements, we train a network of 400 neurons and 40 random groups (see Methods Section 1.9) on each of 100 different target movements independently. (In other words, this generates 100 different gain patterns, with one for each movement.) In Supplementary Fig. 3a, we plot the distribution of gains that we obtain after training across all 100 gain patterns. We plot all 100 outputs from these 100 learned gain patterns in Supplementary Fig. 3b. We also generate 100 new gain patterns by sampling uniformly at random from the distribution in Supplementary Fig. 3a and plot the output of each of these gain patterns in Supplementary Fig. 3c. These

outputs are much more homogeneous than the learned gain patterns in Supplementary Fig. 3b, and they likely would not constitute a good basis set for movement generation.

For library sizes of $l \in \{1, 2, \ldots, 50\}$, we choose 100 samples of l movements (from the learned gain patterns and their outputs) uniformly at random without replacement for each l. We then fit the set of movements in each of the 100 sample libraries using least-squares regression for each of 100 hitherto-untrained novel target movements. We constrain the fitting coefficients c_j from the least-squares regression by requiring that $c_j \geq 0$ for all j and $\sum_{j=1}^{l} c_j = 1$. That is, we consider convex combinations of the coefficients c_j. We calculate the fit error (i.e., the error between the fit and the target), the output error (i.e., the error between the output and the target), and the error between the fit and the output for each of the 100 novel movements, each of the 100 library samples, and each l.

For each l and for each randomly-generated combination of library elements (see the paragraph immediately above), we order the 100 novel target movements based on the error between the output and the fit, and we select the one that is the 50th smallest (i.e., close to the median error). We then extract the output and fit errors for this target and repeat this procedure for each of the 100 randomly-generated combinations of library elements and for $l = 1, \ldots, 50$. We plot these results in Fig. 4c and Supplementary Fig. 3g. In Fig. 4, we plot results for $l \in \{1, 2, \ldots, 20\}$; in Supplementary Fig. 3, we plot results for $l \in \{1, 2, \ldots, 50\}$. Observe that there is only a small change in the errors between $l = 20$ and $l = 50$.

In Fig. 4b, for an example target (and for $l = 2$, $l = 4$, $l = 8$, and $l = 16$), we plot the output and fit that produce the 50th-smallest error between the output and the target across the 100 randomly-generated libraries. In Supplementary Fig. 3e, we calculate the median error over the 100 target movements and we plot the distribution of these median errors over the 100 randomly-generated combinations of library elements for $l = 5$ and $l = 20$.

Additionally, for each l and for each of the 100 target movements, we order the 100 combinations of library elements based on the error between the output and the fit, and we select the one that is the 50th smallest. We then extract the output and fit errors for this combination and repeat this procedure for each of the 100 target movements and for $l = 1, \ldots, 50$. We plot these results in Supplementary Fig. 3h. This indicates that we obtain qualitatively similar results if we average over the 100 target movements or if we instead average over the 100 combinations of library elements. In Fig. 4d and Supplementary Fig. 3d, we first calculate the median error over the 100 target movements for each l and for each of the 100 combinations of library elements. We then plot the median of these errors over the 100 combinations of library elements for each l.

We also calculate the Pearson correlation coefficient between the output and the fit errors for each l when taking the 50th-smallest error across the 100 novel target movements (see Supplementary Fig. 3i) or across the 100 randomly-generated samples (see Supplementary Fig. 3j).

We also repeat these simulations for the baseline rate $r_0 = 5$ Hz in Eqn. (2). We plot the results of these simulations in Fig. 5f (see the next subsection) and Supplementary Fig. 4, and we note that we obtain very similar results to those that we obtained for $r_0 = 20$ Hz.

Simulation details for Figs. 5a–e

We now describe the details of our simulations when using a baseline rate of $r_0 = 5$ Hz.

For the 200-neuron network that we used in Fig. 1, we plot the (relative to baseline) firing rate $f(x)$ (see Eqn. (2)) of 20 excitatory and 20 inhibitory neurons in Fig. 5 with (panel (a)) $r_0 = 20$ Hz in Eqn. (2) and (panel (b)) $r_0 = 5$ Hz. In Fig. 5c, we plot the relative firing rate of all neurons over time versus the relative firing rate when using a linear gain function (i.e., $f(x_i; g_i) = g_i x_i$) for the cases of (black) $r_0 = 20$ Hz and (blue) $r_0 = 5$ Hz. We set all of the gains to 1 for these simulations.

We also train a recurrent neuronal network on the same task as the one that we showed in Figs. 1d–f, except with a baseline rate of $r_0 = 5$ Hz. We plot these results in Fig. 5d–e and compare them to our observations for $r_0 = 20$ Hz. For the 10 noisy initial conditions that we used to generate the outputs in the inset in Fig. 5d, we add white Gaussian noise to the initial condition $\boldsymbol{x}_0$ with a signal-to-noise ratio of 30 dB. In other words, we generate noise in the same manner as we did in Fig. 1f.

Simulation details for Fig. 6 and Supplementary Figs. 5,6,8

We now describe our simulations for learning target activity that lasts longer than 0.5 s. In each of these simulations, we use a network of 400 neurons and 40 random modulatory groups. (See Methods Section 1.9 for details on how we determine such groups.) We construct 'slow' (2.5 s) target movements with $\sigma = 550$ ms and $\ell = 250$ ms in Eqn. (5). We then construct a 'fast' (0.5 s) variant of each movement. Each movement variant has 500 evenly-spaced points (see Methods Section 1.4). We sample the fast variant using 100 evenly-spaced points, and we then augment 400 instances of 0 values to the final 2 s of the movement to ensure that both movement variants have the same length. (See the top right of Fig. 6a.)

Details for Fig. 6b, Supplementary Figs. 5a,c,e, and Supplementary Fig. 8. For Fig. 6b, we fit readout weights using least-squares regression, such that with all gains set to 1, the network output approximates the fast variant. We then train gain patterns using our learning rule in Eqns. (8) and (9) so that the network output generates the slow-movement variant. (The initial condition $\boldsymbol{x}_0$ and readout weights remain fixed.) We use $60,000$ training iterations, and we run 10 independent training sessions for each of 10 different target movements. We plot one such movement in Fig. 6b, and we plot results of all simulations in Supplementary Figs. 5a,c. For Supplementary Fig. 8, we perform the same task except that we scale the amplitude of the slow-movement variant by the factor $1/25$. Scaling the slow-variant target movement by this factor corresponds to the same actual movement but lasting 5 times longer (see Methods Section 1.4). In Supplementary Fig. 8, we show results for the same example that we plotted in Fig. 6b.

Details for Fig. 6c and Supplementary Figs. 5b,d,f,g. We wish to obtain neuronal dynamics that are less sensitive to noisy initial conditions than those that we generated from gain patterns that we obtained from our learning rule (i.e., those that we plot in Supplementary Figs. 5a). For example, in Fig. 6b, the neuronal firing rates have decayed substantially towards baseline after approximately 0.75 s, even though the output activity is close to its maximum value. Therefore, a small change in the initial condition would likely substantially affect the neuronal activity for times after approximately 0.75 s. We therefore perform the task that we described in the paragraph above (i.e., generating a slow-movement variant by changing neuronal gains) using a gradient-descent training procedure with gradients that we obtain from back-propagation [1]. Together with learning the gain pattern for the slow variant, we jointly optimize a single set of readout weights (shared by both the fast-movement and slow-movement variants), as we discussed in Methods Section 1.5, as part of the same training procedure. The gains are still fixed at 1 for the fast variant. The cost function for the training procedure is equal to the squared Euclidean 2-norm between actual network outputs and the corresponding target outputs at both fast and slow speeds plus the Euclidean 2-norm of the readout weights, where the latter acts as a regularizer. We run gradient descent for 500 iterations, which is well after the cost has stopped decreasing.

Using the target movement from Fig. 6b, we plot the output of the back-propagation training procedure in Fig. 6c, and we plot results of all simulations in Supplementary Figs. 5b,d on the same 10 target movements as those that we used in Supplementary Fig. 5a. In Supplementary Fig. 5g, for the outputs in Figs. 6b,c, we add white Gaussian noise with a signal-to-noise ratio of 4 dB to the initial condition. We observe that the outputs from the back-propagation training procedure are less sensitive than the outputs from the learning rule to noisy initial conditions.

Details for Supplementary Figs. 5h–j. In these simulations, we train a single gain pattern that is shared by m different movements, which each last 2.5 s and where each movement corresponds to a different initial condition (IC). To generate a collection of m such ICs, in which each IC evokes neuronal activity of approximately equal amplitude with all gains set to 1, we randomly rotate the top m eigenvectors of the observability Gramian of the matrix $\boldsymbol{W} - \boldsymbol{I}$ [2]. Specifically, we do this by creating a matrix of m columns — one for each of these m eigenvectors — and right-multiplying this matrix by a random $m \times m$ orthogonal matrix (which we obtain via a QR decomposition of a random matrix with elements drawn from a normal distribution with mean 1 and standard deviation 1).

Given m ICs, we uniformly-at-random choose m fast target movements and their slow counterparts out of a fixed set of 10 different movements. We then train a recurrent neuronal network to generate the correct fast and slow target movements by optimizing a single set of readout weights (shared by both fast and slow variants) and a single gain pattern that generates the slow variants (where we set the gains for each of the fast variants to 1). We train using the same gradient-descent method with back-propagation that we described above for Fig. 6c. We plot the results as a function of the number m of movement–IC pairs (see Supplementary Figs. 5h,i) for 10 independent draws of the ICs that we just described above.

Details for Fig. 6d; top panel. For each of the 10 trained movements in Supplementary Figs. 5a,b, we extract the mean minimum error across all simulations for the outputs that we obtain both from our learning rule (see Supplementary Fig. 5a) and from training via back-propagation (see Supplementary Fig. 5b). We then linearly interpolate between the learned gain patterns for the fast and slow outputs, and we and calculate the error (see Methods Section 1.6) between the output and the target movement at the interpolated speed. We calculate these errors for many interpolated movement durations between 0.5 s and 2.5 s, and we plot the mean errors for both our learning rule and the back-propagation training in the top panel of Fig. 6d. We also show an example output that lasts 1.5 s.

Details for Figs. 6d–f and Supplementary Fig. 6. To demonstrate that gain modulation can provide effective smooth control of movement speed for multiple initial conditions of the neuronal activity, we train networks to generate a pair of target movements in response to a corresponding pair of orthogonal initial conditions (see the above description of Supplementary Figs. 5h–j) at fast and slow speeds and also at each of 5 intermediate, evenly-spaced speeds in between these extremes. To do this, we parametrize the gain pattern of speed index s (with $s \in \{1, \ldots, 7\}$) as a convex combination of a gain pattern $\boldsymbol{g}_{s=1}$ for fast movements and a gain pattern $\boldsymbol{g}_{s=7}$ for slow movements, with interpolation coefficients of λ_s (with $\boldsymbol{g}_s = \lambda_s \boldsymbol{g}_{s=1} + (1 - \lambda_s)\boldsymbol{g}_{s=7}$, $\lambda_1 = 1$, and $\lambda_7 = 0$). We optimize (using back-propagation, as discussed above) over $\boldsymbol{g}_{s=1}$, $\boldsymbol{g}_{s=7}$, the 5 interpolation coefficients λ_s (with $s \in \{2, \ldots, 6\}$), and a single set of readout weights. For a given speed s, we use the gain pattern $\boldsymbol{g}_s$ for both movements.

We plot the 7 learned gain patterns in Fig. 6e, and we plot their corresponding outputs for both initial conditions in Supplementary Fig. 6. (We call this collection of 7 trained gain patterns the 'speed manifold'.) We show the linear version of the speed manifold (i.e., interpolating between the fast and slow gain patterns) in Supplementary Fig. 6b. Interpolating between the fast and slow gain patterns accurately generates both movements at any intermediate speed. (See the bottom panel of Fig. 6d.). For both initial conditions, we plot outputs at 5 evenly-spaced speeds by linearly interpolating between the fast ($\boldsymbol{g}_{s=1}$) and slow ($\boldsymbol{g}_{s=7}$) gain patterns in Fig. 6f.

Simulation details for Fig. 7

We simultaneously train gain patterns for controlling different movements (i.e., different movement shapes) and their speed. We train a recurrent neuronal network (using back-propagation, as we discussed previously) to generate each of 10 different movement shapes at 7 different, evenly-spaced speeds (ranging from the fast variant to the slow variant) using a single fixed initial condition $\boldsymbol{x}_0$. To jointly learn gain patterns that control movement shape and speed, we parametrize each gain pattern as the element-wise product of a gain pattern that encodes shape (which we use at each speed for a given shape) and a gain pattern that encodes speed (which we use at each shape for a given speed). We again parametrize (see our details for Figs. 6d–f) the gain pattern that encodes the speed index s (with $s \in \{1, \ldots, 7\}$) as a convex combination of two common endpoints, $\boldsymbol{g}_{s=1}$ (which we use for the fast-movement variants) and $\boldsymbol{g}_{s=7}$ (which we use for the slow-movement

variants). We thus optimize over 10 gain patterns for movement shape, 2 gain patterns each for fast and slow movement speeds, 5 speed-interpolation coefficients (see above), and a single set of readout weights.

In Fig. 7b, we plot the gain patterns that we obtain for controlling the movement speeds at each of the 7 trained speeds. In Fig. 7c, we show the mean error between the network output and the target over the 10 target movements when generating gain patterns for movement speed by linearly interpolating between the trained fast ($\boldsymbol{g}_{s=1}$) and slow ($\boldsymbol{g}_{s=7}$) gain patterns. In Fig. 7d, we plot the outputs of 6 of the 10 gain patterns for movement shape at each of 5 interpolated speeds between the fast and the slow gain patterns. In rightmost panel of Fig. 7a, we plot 2 example movement shapes at 3 interpolated speeds.

Simulation details for Fig. 8 and Supplementary Fig. 7

For these figures, we use the 10 trained gain patterns for movement shapes, as well as the speed manifold from Fig. 7 (see our simulation details for Fig. 7). Using our learning rule from Eqns. (8) and (9), we train 10 coefficients $c_1, \ldots, c_{10}$ (with one for each shape-specific gain pattern; see Fig. 8a) to construct a new gain pattern that, together with the speed manifold, generates a new target movement at the fast and slow speeds. Specifically, we replace the gains g_i (for $i \in \{1, \ldots, N\}$) with the coefficients c_i (for $i \in \{1, \ldots, 10\}$) in Eqns. (8) and (9). We use the mean of the errors at the fast and slow speeds. To generate the network output at the fast and slow speeds, respectively, we calculate the element-wise product between the newly-constructed gain pattern and the fast and slow gain pattern, respectively, on the speed manifold. We independently train, using $10,000$ training iterations, the coefficients $c_1, \ldots, c_{10}$ on each of the 100 target movements that we used for Fig. 4. In Supplementary Fig. 7, we plot histograms of the errors over the 100 target movements after training for both the fast and slow speeds. We plot the mean error (see the black curve) over all 100 target movements at interpolated speeds in Fig. 8c. For the output that produces the 50th-smallest summed errors from fast and slow speeds, we plot the error in red in Fig. 8c. As a control, we calculate the mean error between the network output and the target over the 100 target movements when choosing one of the 100 newly-learned gain patterns uniformly at random without replacement. (See the grey curve in Fig. 8c.)

Additionally, instead of learning to combine gain patterns using the method that we described in the previous paragraph, we determine coefficients $c_1, \ldots, c_{10}$ using a least-squares regression by fitting the 10 learned movements to each of the 100 target movements at the fast and slow speeds simultaneously and requiring that $c_j \geq 0$ for all j and $\sum_{j=1}^{10} c_j = 1$. (See the black dashed curve in Fig. 8c.)

Finally, we plot the Pearson correlation coefficient between pairs of target movements versus the Pearson correlation coefficient between corresponding pairs of learned coefficients $c_1, \ldots, c_{10}$. In our visualization, we plot only $1,000$ of the $4,950$ data points. (We choose these points uniformly at random.) Note that we are unlikely to observe correlation values close to -1 between pairs of combination coefficients because the coefficients $c_1, \ldots, c_{10}$ are likely to sum to approximately 1

(see our discussion of Fig. 4); in fact, we calculate the mean sum of the coefficients to be approximately 0.91.

REFERENCES

1. D. E. Rumelhart, G. E. Hinton, and R. J. Williams, "Learning representations by back-propagating errors," *Nature*, vol. 323, no. 6088, pp. 533–536, 1986.
2. G. Hennequin, T. P. Vogels, and W. Gerstner, "Optimal control of transient dynamics in balanced networks supports generation of complex movements," *Neuron*, vol. 82, no. 6, pp. 1394–1406, 2014.
3. M. M. Churchland, J. P. Cunningham, M. T. Kaufman, J. D. Foster, P. Nuyujukian, S. I. Ryu, and K. V. Shenoy, "Neural population dynamics during reaching," *Nature*, vol. 487, no. 7405, pp. 1–8, 2012.
4. D. Sussillo and L. F. Abbott, "Generating coherent patterns of activity from chaotic neural networks," *Neuron*, vol. 63, no. 4, pp. 544–557, 2009.